Available online at www.sciencedirect.com

ScienceDirect

Green Energy & Environment 9 (2024) 859–876

www.keaipublishing.com/gee

Review article

Potential industrial applications of photo/electrocatalysis: Recent progress and future challenges

Jinhao Li [a], Jing Ren [a], Shaoquan Li [a], Guangchao Li [d], Molly Meng-Jung Li [d,*], Rengui Li [e], Young Soo Kang [f], Xiaoxin Zou [g], Yong Luo [c,*], Bin Liu [a,*], Yufei Zhao [a,b,*]

[a] State Key Laboratory of Chemical Resource Engineering, Beijing University of Chemical Technology, Beijing, 100029, China
[b] Quzhou Institute for Innovation in Resource Chemical Engineering, Quzhou, 324000, China
[c] State Key Laboratory of Organic-Inorganic Composites, Beijing University of Chemical Technology, Beijing, 100029, China
[d] Department of Applied Physics, The Hong Kong Polytechnic University, Hong Kong, 999077, China
[e] State Key Laboratory of Catalysis, Dalian Institute of Chemical Physics, Chinese Academy of Sciences, Dalian National Laboratory for Clean Energy, Zhongshan Road 457, Dalian, 116023, China
[f] Environmental and Climate Technology Track of Korea Institute of Energy, Korea Institute of Energy Technology, Naju-si, Jeollanam do, 58217, Republic of Korea
[g] State Key Laboratory of Inorganic Synthesis and Preparative Chemistry, College of Chemistry, Jilin University, Changchun, 130012, China

Received 7 February 2023; revised 18 April 2023; accepted 6 May 2023
Available online 9 May 2023

Abstract

Nowadays, the rapid development of the social economy inevitably leads to global energy and environmental crisis. For this reason, more and more scholars focus on the development of photocatalysis and/or electrocatalysis technology for the advantage in the sustainable production of high-value-added products, and the high efficiency in pollutants remediation. Although there is plenty of outstanding research has been put forward continuously, most of them focuses on catalysis performance and reaction mechanisms in laboratory conditions. Realizing industrial application of photo/electrocatalytic processes is still a challenge that needs to be overcome by social demand. In this regard, this review comprehensively summarized several explorations in the field of photo/electrocatalytic reduction towards potential industrial applications in recent years. Special attention is paid to the successful attempts and the current status of photo/electrocatalytic water splitting, carbon dioxide conversion, resource utilization from waste, etc., by using advanced reactors. The key problems and challenges of photo/electrocatalysis in future industrial practice are also discussed, and the possible development directions are also pointed out from the industry view.

Keywords: Photocatalysis; Electrocatalysis; Industrial applications; H_2 economy

1. Introduction

With the rapid development of the social economy, excessive fossil energy consumption has caused a global energy crisis and environmental issues (e.g., the greenhouse effect) [1,2]. Photocatalysis and electrocatalysis are regarded to be the most promising technologies for solving the above two issues simultaneously because they can utilize abundant and clean energy [3–6]. Specifically, photo/electrocatalysis can not only convert solar energy or electric energy into green and clean hydrogen energy through water splitting but also convert carbon dioxide (CO_2) into fuels

* Corresponding authors.
E-mail addresses: molly.li@polyu.edu.hk (M.M.-J. Li), luoyong@mail.buct.edu.cn (Y. Luo), liubin@mail.buct.edu.cn (B. Liu), zhaoyufei@mail.buct.edu.cn (Y. Zhao).

https://doi.org/10.1016/j.gee.2023.05.003

and high-value-added chemicals, thus providing solutions for relieving environmental pollution and global warming [7–12].

Photocatalysis uses the endless solar energy existing in nature to be converted into the energy needed by chemical reactions to produce catalysis action [13,14]. It can be divided into three steps: generation of photoinduced electrons–holes from the photocatalyst, separation and transmission of charge carriers, and transfer of surface charge carriers to reactants [15,16]. Different from photocatalytic reactions, electrocatalysis is a catalytic action that accelerates the reaction of charge transfer at the interface between electrode and electrolyte [17–19]. These processes usually involve the adsorption of reactants, diffusion of charge carriers, the reaction of reactants on the surface, and the desorption of products from the electrode surface [20]. Although the energy conversion principles of photocatalysis and electrocatalysis are different, both processes involve the mass transfer and surface-dependent catalysis. There are some similarities in the design strategies for the performance enhancement of catalysts, such as defects engineering, doping, morphology regulation, heterostructure construction, and phases engineering [21–26]. Based on this, a variety of catalysts have been designed and successfully used in a variety of photo/electrocatalytic reactions, and excellent performance has been achieved [27–29]. However, up to now, there are still some bottlenecks in realizing the leap to industrialization. On the one hand, in the laboratory, because the dosage of the catalyst is usually small (only a few grams or milligrams), the cost-effectiveness is inevitably ignored when synthesizing and using the catalyst, which is vital if it is put into industrial application. On the other hand, some special reactors are needed in the practical application process to provide the reaction conditions required by the catalysts. In other words, systematically designing and optimizing devices for different catalytic reactions is worth investigating.

Based on the above reasons, this review systematically summarizes the recent potential and demand to be applied in the industrial practice of photo/electrocatalysis (Fig. 1). The potential industrial applications of representative catalysts in various photo/electrocatalytic processes, such as water splitting and CO_2 conversion under high flow conditions or large current density, are included. Notably, the large-scale integrated processes for holistic renewable energy production and utilization are also highlighted here. The challenges and prospects of photo/electrocatalysts in industrial applications have been prospected. Overall, this review hopes to provide guidelines for the development of industrial applications of photo/electrocatalysis.

2. Wide-scale implementation of solar–driven reaction

At the laboratory stage, some typical photocatalysts have achieved good results in the fields of photocatalytic solar hydrogen production, photocatalytic pollutant removal, and photocatalytic CO_2 conversion. In this section, we will discuss the existing obstacles to practical applications and the current research results of photocatalysts under industrial conditions.

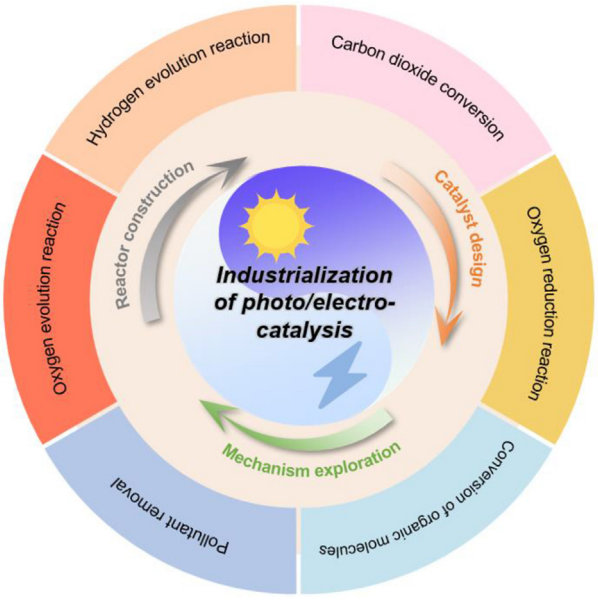

Fig. 1. Schematic diagram showing the photo/electrocatalysis towards potential industrial applications.

2.1. Photocatalytic solar hydrogen production

Fujishima and Honda's research team reported photocatalytic water splitting by TiO_2 semiconductor materials, which reveals the possibility of hydrogen energy generated from light-driven water splitting [30]. The solar photolysis of water mainly uses photocatalysts to absorb light energy. When the photon energy of the incident light is larger than the forbidden band gap energy of the photocatalyst, the electrons in the valence band (VB) will be excited into the conduction band (CB) to produce photo-generated electrons (e^-) and holes (h^+). Then the excited e^- and h^+ migrate from the inside of the catalyst to the surface, where holes oxidize OH^- in water to O_2, and electrons reduce H^+ in water to H_2 [31,32].

It is well known that photocatalysts with industrial application prospects should focus on three factors: (i) low production cost; (ii) carrier generated by photocatalyst can be quickly separated; (iii) an appropriate band gap to support as much solar spectrum utilization as possible (like can absorb light above 550 nm) [33–36]. Although the industrialization of photocatalytic hydrogen production is in the primary research stage, with the continuous in-depth exploration of researchers, some attempts from the laboratory scale to the wide-scale application have been reported. Domen et al. [37] used 1600 panel reaction units and gas separation equipment (recovering membrane separation technology) to establish a 100 m^2 scale photocatalytic water decomposition hydrogen production system (Fig. 2 (a)). The reactor is expected to realize photocatalytic water decomposition on a large scale, and the maximum solar-to-hydrogen efficiency is 0.76%. Recently, Takanabe et al. [38] considered that some factors (change of temperature difference between day and night, water flow, etc.) would inevitably cause problems such as the shedding of

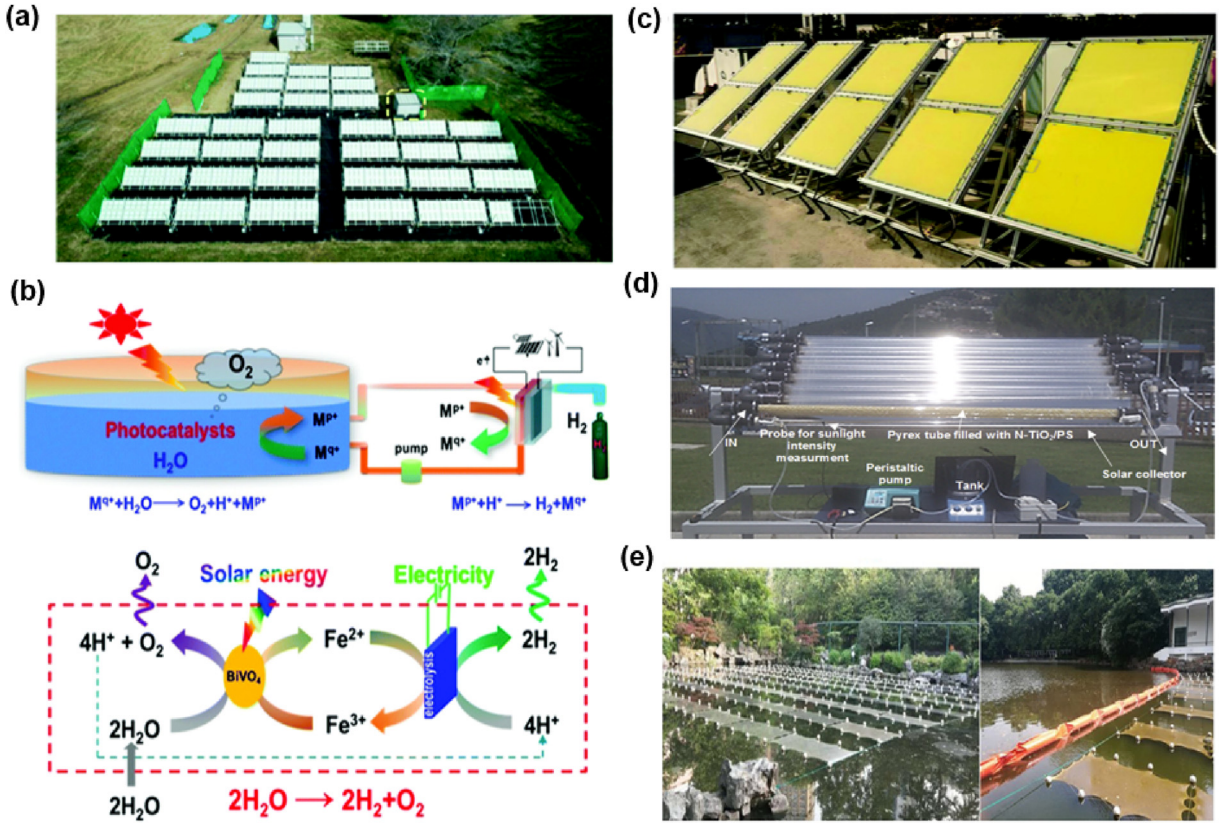

Fig. 2. (a) The 100 m^2 array of panel reactors for solar hydrogen production (Reprinted with permission from Ref. [37] Copyright (2021) Springer.). (b) Scheme of scalable water splitting using particulate photocatalysts via HFP. (c) Picture of the demonstration module for large-scale solar energy storage (Reprinted with permission from Ref. [39] Copyright (2020) Wiley.). (d) The pilot scale solar photoreactor for water treatment (Reprinted with permission from Ref. [47] Copyright (2018) Elsevier.). (e) The solar-active cloths for wastewater treatment (Reprinted with permission from Ref. [48] Copyright (2019) Elsevier.).

photocatalysts and the dissolution of ions in catalysts and cocatalysts. In addition, finding a milder way to replace the water flow and reduce the external corrosion of the catalyst is also a consideration in practical application. Given this, they made an exploratory study: Al-doped $SrTiO_3$-based photocatalyst decorated homogeneously with nanomembrane TiO_x or TaO_x thin layers (<3 nm) were successfully prepared, and the apparent quantum efficiency of this material is 54 ± 4% with water vapor as a water source (this efficiency can be maintained under the condition of 0.3 MPa). This concept of steam feeding is innovative as a high-pressure and light-resistant reactor and may be valuable for the further development of large-scale applications of photocatalysis. Nevertheless, there are still challenges in practical application. For example, the membrane separation method used to separate the mixed gas of H_2 and O_2 leads to insufficient separation of H_2, which may cause safety hazards. If reactors are scale-up, the key problem is to seal them to prevent any gas leakage, but this may increase the cost and technical difficulties of industrial utilization. The simultaneous generation of H_2 and O_2 gases may lead to explosions. Facing the above challenges, Li's group inspired by the principle of natural photosynthesis and referring to the idea of planting crops on a large scale on a farm, took the lead in proposing and verifying a hydrogen farm project (HFP) (Fig. 2 (b)) [39]. The HFP consists of two sub-systems, one is photocatalytic water oxidation to capture solar energy to generate e^- and h^+, and utilize this to produce H_2. In the whole process, only H_2 was generated, thus avoiding the need for H_2/O_2 separation. Specifically, using well-defined $BiVO_4$ crystals as photocatalysts, the quantum efficiency of photocatalytic water oxidation is as high as 71% by adjusting the exposure ratio of its oxidation and reduction reaction crystal planes and using Fe^{3+}/Fe^{2+} as electronic mediators. The solar-to-hydrogen efficiency over 1.8% could be achieved. The reverse reaction between H_2 and O_2 is avoided in the whole process, which can solve the technical bottleneck of large-scale application of photocatalytic water oxidation reactor. Importantly, they continued to expand the system, set up an enlarged experimental device under sunlight irradiation outdoors, and verified the feasibility of the HFP (Fig. 2 (c)).

It is worth noting that the application of photocatalytic technology to organic synthesis is a new field with great potential for industrial application in photocatalytic research [40]. In some typical reactions, photocatalytic dehydrogenation and oxidation of organic matter can not only realize the directional conversion of organic matter but also produce hydrogen, which can be seen as an economic and green reaction. Wu et al. [41] used CdSe quantum dots (QDs) as a photocatalyst to realize the alkylation and arylation of allylic C (sp^3)–H bond with H_2 evolution. The availability of multiple

binding sites allows e^- and h^+ acceptors to combine with QDs at the same time, so as not to accumulate excessive charges on the photocatalyst, which makes the reaction have impressive efficiency and selectivity for the synthesis of high-valuable organic species. In another work [42], they also selected quantum dots as photocatalysts, and for the first time realized the efficient and selective thiol reaction of allylic C (sp^3)–H or vinylic C (sp^2)–H, accompanied by the release of H_2, provides a new route on the not only H_2 evolution but also organic synthesis.

2.2. Photocatalytic pollutant removal

Photocatalysis is considered an important treatment scheme for industrial wastewater remediation. To shift laboratory-scale research to pilot-scale or full-scale operation, researchers have made lots of efforts, and reports on photocatalytic removal of different types of pollutants (dyes, phenolic compounds, metal ions, etc.) [43,44]. Generally speaking, the exploration in this field usually focuses on three aspects: (i) the photoactivity of the catalyst is changed or the degradation rate in the visible range is increased; (ii) the recovery and deactivation of photocatalyst; (iii) the enlargement of the reactor and the optimization of process parameters [45,46]. Vaiano et al. [47] studied the application of a packed-bed solar photocatalytic reactor in the advanced treatment of municipal sewage based on visible light active N-doped TiO_2 photocatalyst. Firstly, a series of photocatalytic tests were conducted in a laboratory-scale reactor, and it was found that the photocatalyst did not show deactivation after several treatment cycles. Subsequently, outdoor experiments were carried out using a reactor based on a solar composite triangular collector (Fig. 2 (d)). The results showed that the photocatalyst achieved an efficient water treatment effect under direct sunlight, and the removal rate of local *Escherichia coli* was up to 87% after 120 min of treatment. Chen and Huang et al. [48] designed and synthesized BT/3DG catalyst by immobilizing black titania (BT (TiO_{2-x})) on the 3D graphene (3DG) substrate. To realize its industrial application, they bonded BT/3DG hybrids to non-woven cloth through a polymer binder to obtain a solar-active cloth, which has buoyancy and can float on water. Subsequently, it was used in wastewater remediation tested on the field in polluted rivers and ponds (Fig. 2 (e)). Generally, after two weeks of cloth spreading, it is measured that the total organic carbon, nitrogen, and phosphorus components of the treated water decrease significantly, and the appearance of the water changes remarkably. Therefore, this kind of solar-active cloth is not only beneficial to advanced oxidation processes but also can complete water remediation by itself. Baaloudj and Badawi et al. [49] chose sillenite $Bi_{12}TiO_{20}$ (BTO) as the catalyst and studied the photocatalytic removal efficiency of several typical antibiotics, namely cefixime (CFX), cefaclor (CFC), and cefuroxime (CFRM). The BTO showed excellent removal efficiency of CFX, CFC, and CFRM was 94%, 81%, and 69.71%, respectively, within 210 min. Subsequently, the batch test results prove the feasibility of using BTO sillenite as a sustainable and cost-effective photocatalytic system in the wide-scale demonstration of pharmaceutical wastewater treatment. Notably, photocatalytic technology has also shown amazing potential in large-scale air purification. Using renewable solar energy, volatile organic compounds (VOCs) can be efficiently removed and degraded under mild reaction conditions. A single-pass semi-industrial photocatalytic oxidation reactor has been designed by Thevenetc's group [50]. They studied the photocatalytic oxidation removal of isopropanol under industrial conditions (high isopropanol concentrations and airflow rates). They show that compared with other treatment technologies, this technology has many advantages in operating costs and can be regarded as an efficient technology to deal with industrial emissions. Shu et al. [51] designed and synthesized the trifunctional catalyst Mn/TiO_2/ZSM-5, and used it to degrade toluene and ethylacetate in photocatalytic oxidation. After achieving a good removal effect at the laboratory level, it was further expanded to the pilot scale, which confirmed the possibility of popularizing this technology for practical application. As a whole, to fully realize the application of photocatalysis pollutant removal in industry, there are still some limitations that cannot be ignored. Due to low quantum yield and easy recombination of photogenerated e^- and h^+, it is difficult to deal with large amounts of industrial waste gas and wastewater, and can only be used to degrade low-concentration organic pollutants.

2.3. Photocatalytic CO_2 conversion

Photocatalytic technology is used to convert CO_2 into valuable hydrocarbon fuel, which provides a new means to realize carbon recycling. The photocatalytic CO_2 conversion process mainly includes photon absorption, photogenerated electrons (e^-)–holes (h^+) separation and transportation, and surface CO_2 reduction reactions [52,53]. Specifically, when the photocatalysts are illuminated by the light with photon energy higher than the band gap, e^- in the valence band are excited to the conduction band, thus forming e^-–h^+ pairs. After that, the e^-–h^+ pairs are separated and migrated, reaching the catalytically active sites on the surface of the photocatalyst and participating in the subsequent catalytic reaction. Finally, these formed products are desorbed from the surface of the photocatalyst. At present, the photocatalytic reduction of CO_2 to various products including CO, CH_4, CH_3OH, etc. has been widely reported (as shown in Fig. 3(a)), and a large number of photocatalysts have been proven to have the decent activity and selectivity. For example, our group [29] used a monolayer MgAl layered double hydroxides (mMgAl-LDH) for realizing super-stable mineralization of multiple heavy metal ions (like Ni, and Cu ions), and found that Ni^{2+} replaced the Mg^{2+} sites within the catalyst layers to form NiMgAl-LDH, and Cu^{2+} was fixed on the surface of the catalyst with high dispersibility to form CuMgAl-LDH. When the NiMgAl-LDH was used as a photocatalyst for CO_2 conversion, the high selectivity of CO and CH_4 was exhibited (Fig. 3 (b)). In addition, CuMgAl-LDH can be further used for

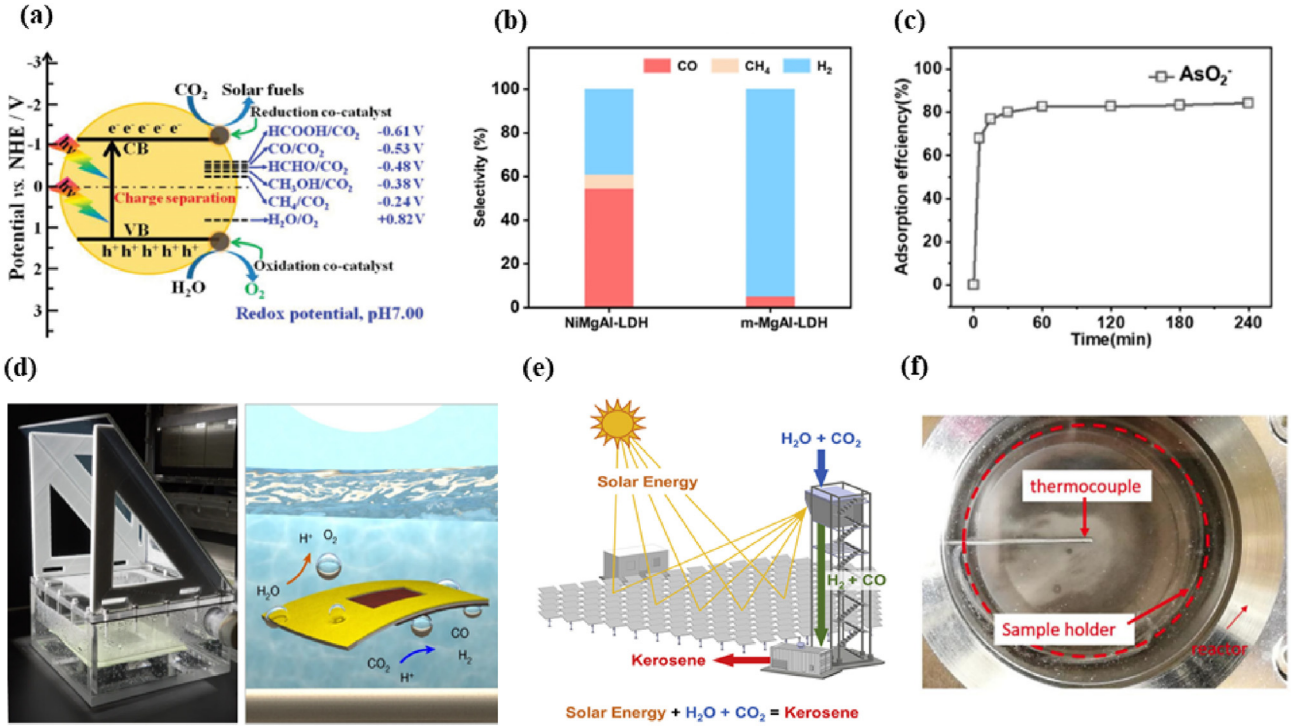

Fig. 3. (a) The schematic diagram of photocatalytic reduction of CO_2 to various valuable products (Reprinted with permission from Ref. [53] Copyright (2016) ACS.). (b) Photocatalytic CO_2 reduction product selectivity of NiMgAl-LDH and (c) adsorption efficiency of CuMgAl-LDH for AsO_2^- (Reprinted with permission from Ref. [29] Copyright (2022) Elsevier.). (d) Set-up employed to characterize large-scale floating leaves (Reprinted with permission from Ref. [56] Copyright (2022) Springer.). (e) Overview of installed solar tower plant (Reprinted with permission from Ref. [57] Copyright (2022) Cell Press.). (f) The digital image of the reactor with a thermocouple (Reprinted with permission from Ref. [58] Copyright (2018) Wiley.).

removing anions from sewage, and the removal efficiency can reach more than 80% (Fig. 3 (c)). However, the current conversion efficiency and selectivity are insufficient to meet the requirements of practical application, and it is usually necessary to combine photothermal and photoelectric strategies to overcome many obstacles that hinder the large-scale application of photocatalytic CO_2 reduction in the industry [54,55]. With the deepening of research, some industrial-scale attempts have been made. A recent study by Reisner et al. [56] showed that the lead halide perovskite photocathodes deposited onto indium tin oxide-coated polyethylene terephthalate achieved an activity of 4266 $\mu mol\, H_2\, g^{-1}\, h^{-1}$ using a Pt catalyst. Excellent solar-to-fuel efficiencies are demonstrated in the corresponding lightweight perovskite-$BiVO_4$ PEC devices, with H_2 of 0.58% and CO of 0.053%. Subsequently, they expanded it into 100 cm^2 stand-alone artificial leaves, and its sustained comparable performance and stability were comparable to those of the same kind with 1.7 cm^2 counterparts. In operation, the 30–100 mg cm^{-2} device can float due to the formation of bubbles, which is beneficial to collect gas on the river and is more convenient for practical application (as shown in Fig. 3 (d)). Koepf et al. [57] achieved the cracking of H_2O and CO_2 was performed via a ceria-based thermochemical redox cycle to produce a tailored mixture of H_2 and CO (syngas) with full selectivity, which was further processed to kerosene (Fig. 3 (e)). Without applying heat recovery, the energy conversion efficiency from solar to syngas was 4.1%. The operation of this solar tower fuel plant is closely related to industrial implementation and has a guiding role in sustainable aviation fuel production. Bai et al. [55] put forward the concept of liquid sunshine, the connotation of which is to use renewable energy to water splitting to produce hydrogen, and then synthesize fuel molecules (methanol) from hydrogen and CO_2 under the action of a catalyst. This technology has the advantages of large-scale energy storage, hydrogen storage, and direct resource conversion and utilization of CO_2. After continuous exploration, this technology entered a new stage of industrialization. As a matter of fact, besides CO_2, other small molecules (such as CO) can be converted into high-value products by using sunlight energy, which is also considered to have certain potential in industrial applications. Zhao et al. [58] successfully prepared a series of Fe-based heterogeneous photocatalysts by reducing ZnFeAl-LDH nanosheets with H_2 at a certain temperature. At the reduction temperature of 500 °C, the heterogeneous photocatalyst showed impressive hydrogenation performance of CO hydrogenation, with initial selectivity of 89% to hydrocarbons, especially light olefins (42%) and low selectivity to CO_2 (11%) under batch or flow reactor tests (Fig. 3 (f)). At present, the field of photocatalytic CO_2 conversion is at a critical stage from laboratory to industrial application, which needs attention from two aspects: (i) the conversion efficiency and the selectivity of target products can be improved by designing and synthesizing high-efficiency catalysts; (ii) the research on photocatalytic conversion can be actively promoted by developing a reactor with reasonable design and optimizing this process.

3. Electrocatalytic reaction with current density at industrial-level

For industrial applications, to achieve high production efficiency, various electrocatalytic reactions are often carried out under large current densities. However, up to now, the current of the catalytic reaction is usually below 100 mA cm^{-2}, which is still far from the industrialization standard and cannot meet the requirements of industrialization. In this section, with the help of some representative catalysts, we mainly introduce the catalytic performance and possible reaction mechanism of several typical electrocatalytic reaction types at industrially-relevant current density.

3.1. Electrocatalytic water splitting

Electrocatalytic water splitting can be producing high-purity hydrogen and oxygen, which mainly includes two half-reactions, namely hydrogen evolution reaction (HER) at the cathode and oxygen evolution reaction (OER) at the anode [59].

Among the current water electrolysis technologies, alkaline water electrolysis (AEL) and proton exchange membrane water electrolysis (PEMWE) are relatively mature. The test criteria condition of AEL in industrial applications usually includes KOH as the electrolyte, an operating temperature of approximately 80 °C, and a generated gas pressure of 0.1–3.0 MPa [60]. To ensure the separation of reaction products (mainly hydrogen and oxygen), a diaphragm needs to be set between the anode and cathode of the electrolyzer [61]. Unfortunately, the problems of alkaline solution loss, corrosion, and high energy consumption are still difficult to overcome for AEL, hampering its further large-scale application. PEMWE is different from AEL, and it uses the proton exchange membrane as solid electrolyte instead of diaphragm and liquid electrolyte, which makes it have excellent safety, and higher current density [62]. Generally, the cost and working efficiency of these two technologies are closely related to the activity and stability of electrocatalysts used in the anode (OER electrocatalysts) and cathode (HER electrocatalysts).

Two electron transfer processes are involved in HER occurring on the cathode, including Volmer/Heyrovsky step or Volmer/Tafel step. Depending on the reaction medium, H_2 can be generated by the reduction of H^+ (acidic condition) or H_2O (alkaline condition), and the process is as follows [63,64].

In acidic electrolyte, the first step is the adsorption of H^+ on the catalyst surface to form adsorbed hydrogen atom (H*).

$$H^+ + e^- \rightarrow H^* \text{ (Volmer step)} \quad (1)$$

Then the second step is the formation of hydrogen molecules through the electrochemical route (H* combines with H^+ and e^- to form a hydrogen molecule);

$$H^* + H^+ + e^- \rightarrow H_2 \text{ (Heyrovsky step)} \quad (2)$$

or the chemical path (two H* on the catalyst surface combine to form a hydrogen molecule).

$$2H^* \rightarrow H_2 \text{ (Tafel step)} \quad (3)$$

Under alkaline conditions, due to the lack of H^+, HER starts from the decomposition of H_2O to provide H^+.

$$H_2O + e^- \rightarrow H^* + OH^- \text{ (Volmer step)} \quad (4)$$

$$H_2O + e^- + H^* \rightarrow OH^- + H_2 \text{ (Heyrovsky step)} \quad (5)$$

$$2H^* \rightarrow H_2 \text{ (Tafel step)} \quad (6)$$

To date, great efforts have been made to synthesize large current-based HER catalysts and show the value of potential industrial applications. These catalysts inevitably have four major structural characteristics, including hydrophilic physical structure, high active site density, remarkable intrinsic catalytic activity, and outstanding conductivity of the substrate [65]. Two-dimensional layered materials, represented by MoS_2 and WS_2, are well-known as advanced electrocatalysts for HER under high current density [66]. Compared with some bulk materials, this kind of material has more exposed edges and can expose abundant active sites. As depicted in Fig. 4 (a), Liu et al. [67] combined Mo_2C nanoparticles and MoS_2 (after exfoliation) with the carrier by spraying and dipping technology and obtained the electrocatalyst after further thermal treatment (named HC-MoS_2/Mo_2C). This material exhibits excellent HER activity and requires small overpotentials of 412 mV (0.5 mol L^{-1} H_2SO_4 solutions) and 441 mV (1 mol L^{-1} KOH solutions) to achieve the 1000 mA cm^{-2}. Then, they produce electrocatalysts via the lower-cost molybdenum natural resources (molybdenite mineral) as raw materials through the same strategy. The test displayed that these electrocatalysts also have good electrocatalytic performance and show superior stability at high current density. It has been proved that the edge sulfur sites of crystalline MoS_2 have catalytic activity for HER, but a large number of sulfur atoms in the substrate plane are inert, which usually leads to difficulty in further improving the catalytic activity of the catalyst. In contrast, materials with amorphous structures have been proven to be a better catalytic performance for HER than their crystalline counterparts because of their abundant active sites. Given this, Zhang et al. [68] creatively synthesized amorphous molybdenum tungsten S/N-doped reduced graphene oxide nanocomposites (a-$MoWS_x$/N-RGO), which can easily reach 1000 mA cm^{-2} current densities with 348 mV overpotentials. The relevant DFT calculation reveals that the extra electrons are preferentially filled at active site (two S^{2-}), which leads to the high activity of two S^{2-} under the condition of electrons injection, revealing the reason for extraordinary HER activity under high current density conditions. In fact, several metal complexes (metal nitrides, metal phosphides, and metal oxides) with higher intrinsic activity also show excellent HER performance. For instance, Jiang et al. [69] synthesize a $Ni_{0.2}Mo_{0.8}N$ grown on Nickel foam (NF), which can exhibit the overpotential of 70 mV to derive the 300 mA cm^{-2} in an alkaline medium. Li et al. [70] proposed a strategy of surface self-reconstruction of Cu–Fe_3O_4 by electrochemical activation to promote its HER performance. In the

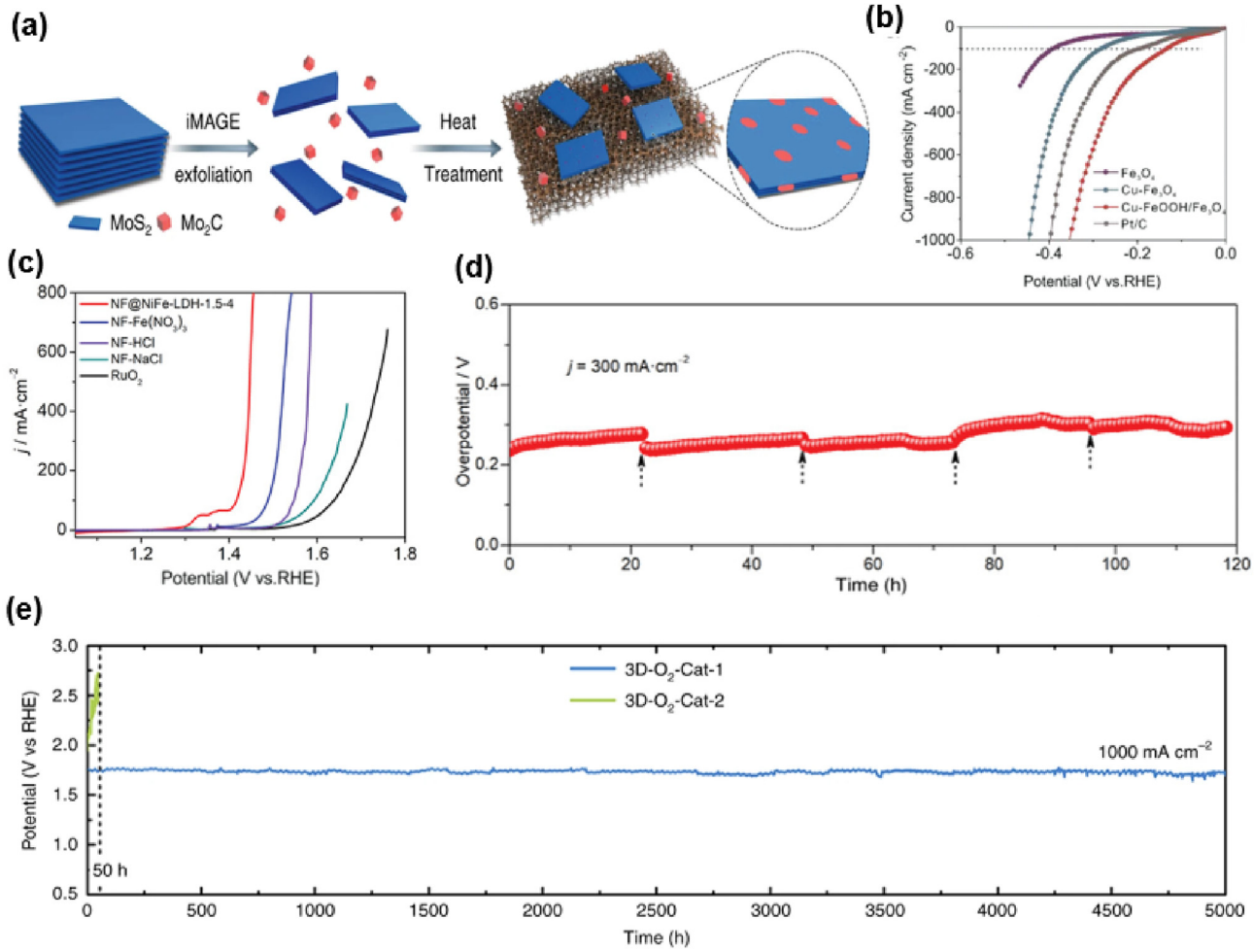

Fig. 4. (a) Schematic of the synthetic route for the MoS_2-based ink-type electrocatalyst (Reprinted with permission from Ref. [67] Copyright (2020) Springer.). (b) LSV curves of Cu-FeOOH/Fe_3O_4 catalyst for the HER performance (Reprinted with permission from Ref. [70] Copyright (2022) Wiley.). (c) The OER performance and (d) long-term durability measurement of NiFe-LDH nanosheet arrays on Ni foam electrocatalyst (Reprinted with permission from Ref. [76] Copyright (2022) Wiley.). (e) Chronopotentiometric curve of catalytic in 1 mol L^{-1} KOH at a current density of 1000 mA cm^{-2} (Reprinted with permission from Ref. [78] Copyright (2018) Springer.).

HER process, the surface of the catalyst will produce defective FeOOH due to the stimulation of applied potential, following a "dissolution-redeposition" path. The resulting electrocatalysts (Cu–FeOOH/Fe_3O_4) display excellent alkaline HER performance with an overpotential of 285 mV at 500 mA cm^{-2} (Fig. 4(b)). Dong et al. [71] found that with the assistance of the high valence Mo to adjust the local electronic configuration and atomic arrangement, the prepared Mo–CoP/MoO_x sample shows low overpotentials of 226 mV to reach large than 2000 mA cm^{-2} in alkaline solution.

The OER has a more complex reaction pathway than HER, which is a four-electron transfer process, and the reaction kinetics is slow. Similar to HER, the mechanism of OER is closely related to the reaction medium, which involves a variety of surface-adsorbed reaction intermediates, such as M−OH, M−O, and M–OOH (M represents the active site on the catalyst surface), as described in the following [72,73].

In acidic electrolyte, M first combines with H_2O to form M–OH.

$$M + H_2O \rightarrow M{-}OH + H^+ + e^- \quad (7)$$

Then, M−OH removes an H^+ to form M–O. M−O may generate O_2 through two different reaction paths. One is that two adjacent M−O directly generate O_2, and the other is that M−O combines with water to form M–OOH, which generates O_2 and M.

$$M{-}OH \rightarrow M{-}O + H^+ + e^- \quad (8)$$

$$2M{-}O \rightarrow 2M + O_2 \quad (9)$$

$$M{-}O + H_2O \rightarrow M{-}OOH + H^+ + e^- \quad (10)$$

$$M{-}OOH \rightarrow M + O_2 + H^+ + e^- \quad (11)$$

Under alkaline conditions, M combines with OH^- to form M–OH.

$$M + OH^- \rightarrow M{-}OH + e^- \quad (12)$$

Further, M−OH combines with OH^- to generate H_2O and M−O intermediates. There may also be two reaction paths in this step.

$$M-OH + OH^- \rightarrow M-O + H_2O + e^- \quad (13)$$

$$2M-O \rightarrow 2M + O_2 \quad (14)$$

$$M-O + OH^- \rightarrow M-OOH + e^- \quad (15)$$

$$M-OOH + OH^- \rightarrow M + O_2 + H_2O + e^- \quad (16)$$

Ni-based compounds are regarded as the most promising electrocatalyst for OER. This is mainly because these compounds have appropriate chemical adsorption free energy for the formed intermediates, which is second only to precious metal-based materials and may show smaller theoretical overpotential [74]. Recent research has found that NiOOH with high Ni valence in Ni-based compounds is usually thought of as the catalytic active center of OER. If Fe^{3+} exists, its electronic effect can further promote the formation of NiOOH, thus accelerating the catalytic reaction [75]. Inspired by the above viewpoint, the leading OER catalysts with excellent performance reported at present are mainly NiFe-based compounds, and their activity is further improved by crystal structure design and adjustment of the chemical composition. Xu and Hou et al. [76] prepared NiFe-LDH nanosheet arrays on Ni foam by methods of the one-step solution-phase etching, which only required overpotentials of 220 mV to obtain 657 mA cm^{-2} current density in alkaline (Fig. 4 (c)). Thanks to the pores formed by nanosheet arrays, it can effectively increase available active sites and reduce ion diffusion distance/transmission resistance. Meanwhile, the close combination of NiFe-LDH and NF enhances the stability and mechanical properties of the prepared catalyst (Fig. 4 (d)). More recently, Zou and co-workers further realized the commercial-scale application of NiFe-based catalysts [77]. They designed and fabricated sulfurated stainless steel meshes, and expanded to obtain m^2-sized NiFe-based electrodes. It was found that when it was integrated into an industrial alkaline electrolyzer, its OER performance was even far superior to that of the Raney nickel electrode electrolyzer at the same working temperature (80 °C) and electrolyte concentration (30% KOH), which can reach 300 mA cm^{-2} with a stability of 120 h. In their other work [78], by adjusting the corrosion reaction of the iron substrate at room temperature and optimizing the corrosion products of iron, a high-activity OER catalytic material was obtained. The catalytic material can work stably for more than 8 months under the current of 1000 mA cm^{-2} (Fig. 4 (e)). In addition to NiFe-based catalysts, metal phosphides and metal oxides are another class of excellent OER electrocatalysts. For example, Lu et al. [79] designed an N-doped C/Ni_5P_4/Fe_3P hollow nanocubes electrode, which has excellent OER performance with overpotentials were 385 mV at the current density of 250 mA cm^{-2}. Li et al. [80] have prepared a one-dimensional linear structure Co_3O_4/$Fe_{0.33}Co_{0.66}P$/NF. This material exhibits an overpotential of 291 mV at 800 mA cm^{-2}. It is worth noting that a variety of bifunctional catalysts that can drive a large current density in overall water splitting (OER and HER) have been developed, which is of great significance for effectively reducing device fabrication costs. For instance, Ye et al. [81] designed monolithic three-dimensional hollow foam electrodes (Ni–Mo–B HF) by combining electroless plating with calcination. Beneficial from the unique structure, when this electrocatalyst was used in a two-electrode configuration directly, it achieved a current density of 450 mA cm^{-2} at a low cell voltage of 1.8 V, together with long-term stability. Tang and co-workers synthesized Mo_2S_3@$NiMo_3S$ with metallic heterojunction, which showed low overpotentials of 390 and 174 mV with a current density of 1000 mA cm^{-2} for HER and OER, respectively [82]. When used as the cathode and anode, it only needed 1.675 V to achieve 1000 mA cm^{-2}. Yin's group prepared a carbon-encapsulated $FeWO_4$–Ni_3S_2 using the solvothermal and calcination method, which was used to assemble the overall water splitting device, presenting outstanding durability for 100 h at 1000 mA cm^{-2} in harsh simulated industrial conditions (6.0 mol L^{-1} KOH, 60 °C) [83]. Very recently, Zhang et al. [84] fabricated amorphous Mo-doped $NiS_{0.5}Se_{0.5}$ nanosheets@crystalline $NiS_{0.5}Se_{0.5}$ nanorods by a simple hydrothermal strategy. Benefitting from the amorphous structure with a high density of unsaturated sites, when utilizing the full-cell water splitting, it delivered the low cell voltage of 1.98 V to realize the large current density of 1000 mA cm^{-2}. At present, there are many catalysts for electrocatalytic water splitting with high current density in alkaline electrolytes, but there are few reports in acidic or seawater electrolytes. Therefore, it is highly desirable to design and develop catalysts suitable for acidic or seawater environments by improving the resistance to corrosion and stability of catalysts under extreme conditions.

3.2. Electrocatalytic conversion of organic molecules

Although a variety of high-efficiency OER and HER catalysts have been developed to reduce the overpotential in the reaction process under commercially functional current density, there are still some problems that need to be solved urgently: (i) the product of anode is O_2, which has low value and is easy to mix with H_2 in the electrolytic cell; (ii) the OER process usually requires high energy consumption, and its slow kinetics seriously hinders industrial water splitting even under the action of the catalyst. Under this scenario, a thermodynamically more favorable strategy of electrocatalytic conversion of organic molecules instead of OER has been proposed. Compared with traditional water splitting, this strategy can not only significantly reduce the working voltage to produce hydrogen but also oxidize organic molecules at the anode to obtain some high-value-added compounds, thus improving the economic benefits [85]. Table 1 lists the HER, OER, and electrocatalytic conversion of organic molecules performances of a series of reported electrocatalysts.

The nitrogen-containing small molecules (urea, hydrazine) have low theoretical oxidation potential, which appealing alternative to OER. Urea is a major pollutant that causes the

Table 1
Comparison of the electrocatalytic activities of various electrocatalysts for HER, OER, and electrocatalytic conversion of organic molecules under high current density.

Electrocatalysts	Reaction types	Electrolyte	Performance	Ref.
HC-MoS_2/Mo_2C	HER	1.0 mol L^{-1} KOH	Overpotential 441 mV @ 1000 mA cm^{-2}	[67]
a-$MoWS_x$/N-RGO	HER	1.0 mol L^{-1} KOH	Overpotential 348 mV @ 1000 mA cm^{-2}	[68]
$Ni_{0.2}Mo_{0.8}N$/Ni	HER	1.0 mol L^{-1} KOH	Overpotential 70 mV @ 300 mA cm^{-2}	[69]
Cu−FeOOH/Fe_3O_4	HER	1.0 mol L^{-1} KOH	Overpotential 285 mV @ 500 mA cm^{-2}	[70]
Mo−CoP/MoO_x	HER	1.0 mol L^{-1} KOH	Overpotential 226 mV @ 2000 mA cm^{-2}	[71]
NF@NiFe-LDH-1.5-4	OER	1.0 mol L^{-1} KOH	Overpotential 220 mV@ 657 mA cm^{-2}	[76]
MS/SS	OER	30% KOH	Overpotential 307 mV @ 100 mA cm^{-2}	[77]
3D-O_2-Cat-1	OER	1.0 mol L^{-1} KOH	Overpotential 340 mV @ 1000 mA cm^{-2}	[78]
N-doped C/Ni_5P_4/Fe_3P	OER	1.0 mol L^{-1} KOH	Overpotential 385 mV @ 250 mA cm^{-2}	[79]
Co_3O_4/$Fe_{0.33}Co_{0.66}P$	OER	1.0 mol L^{-1} KOH	Overpotential 291 mV@ 800 mA cm^{-2}	[80]
$Ni_{12}P_5$/Ni-Pi/NF	UOR	1.0 mol L^{-1} KOH/0.5 mol L^{-1} urea	Potential 1.378 V @ 900 mA cm^{-2}	[86]
Ni−Co_2VO_4/NF	UOR	1.0 mol L^{-1} KOH/0.5 mol L^{-1} urea	Potential 1.45 V @ 1000 mA cm^{-2}	[87]
MnO_2/$MnCo_2O_4$/Ni	UOR	1.0 mol L^{-1} KOH/0.5 mol L^{-1} urea	Potential 1.7 V @ 1000 mA cm^{-2}	[88]
Ni_xFeN/Ni_3N	UOR	1.0 mol L^{-1} KOH/0.5 mol L^{-1} urea	Potential 1.372 V @ 500 mA cm^{-2}	[89]
Fe_2P@Ni_xP/NF	UOR	1.0 mol L^{-1} KOH/0.5 mol L^{-1} urea	Potential 1.4 V @ 800 mA cm^{-2}	[90]
Ni_2P/NF	HzOR	1.0 mol L^{-1} KOH/0.5 mol L^{-1} hydrazine	Potential 18 mV @ 200 mA cm^{-2}	[91]
$FeWO_4$-WO_3/NF	HzOR	1.0 mol L^{-1} KOH/0.5 mol L^{-1} hydrazine	Potential 0.164 V @ 1000 mA cm^{-2}	[92]
h-NiSe/CNTs	MOR	1.0 mol L^{-1} KOH/1.0 mol L^{-1} methanol	Potential 1.65 V @ 400 mA cm^{-2}	[95]
Ni_3S_2-CNFs/CC	MOR	1.0 mol L^{-1} KOH/1.0 mol L^{-1} methanol	Potential 1.74 V @ 1000 mA cm^{-2}	[96]
Au/CoOOH	AOR	1.0 mol L^{-1} KOH/0.1 mol L^{-1} benzyl alcohol	Potential 1.5 V @ 540 mA cm^{-2}	[97]
$Co_{0.4}$NiS@NF	HMFOR	1.0 mol L^{-1} KOH/50 × 10^{-3} mol L^{-1} HMF	Potential 1.45 V @ 497 mA cm^{-2}	[99]

eutrophication of water resources, and it is a very meaningful work by electrochemical oxidation into N_2 and CO_2 at the industrial level. As shown in Fig. 5 (a), Huang's group constructed a bifunctional self-supporting electrocatalyst comprising of Ni phosphate-anchored $Ni_{12}P_5$ nanorod arrays grown on NF ($Ni_{12}P_5$/Ni-Pi/NF) [86]. When used as anode catalysts for urea oxidation reaction (UOR), it exhibited rather low potentials of 1.358 V (500 mA cm^{-2}) and 1.378 V (900 mA cm^{-2}) in 1.0 mol L^{-1} KOH with 0.5 mol L^{-1} urea (Fig. 5 (b)). In addition, the electrode also showed significant HER catalytic activity, and it has rather low potentials of 0.312 V at 500 mA cm^{-2}. These high catalytic activities make the two-electrode electrolyzer composed of UOR and HER have excellent cell performance, capable of delivering 500 mA cm^{-2} at a voltage of 1.662 V. The excellent performance of the $Ni_{12}P_5$/Ni-Pi/NF could be ascribed to its unique porous network structures of NF, abundant defects in the Ni phosphate shell, and the high specific surface area of the catalyst. Also, the combination of 3D substrate and a well-arranged 1D nanorod array can effectively promote the diffusion of electrolyte ions and the dissipation of generated bubbles, and promote the improvement of catalytic performance. Yin et al. [87] used the hydrothermal method and calcination strategy to grow the Ni–Co_2VO_4 nanosheet array on NF (Ni–Co_2VO_4/NF). The heterojunction interface between Ni and Co_2VO_4 leads to the redistributing of the charge to form poor/rich-electrons species, which can further promote the adsorption of urea molecules and H_2O, thus enhancing the catalytic activity. Specifically, Ni–Co_2VO_4/NF could need a small potential of 1.45 V and 329 mV to reach large current densities (1000 mA cm^{-2}) for UOR and HER, respectively. Remarkably, using Ni–Co_2VO_4/NF as the anode and cathode

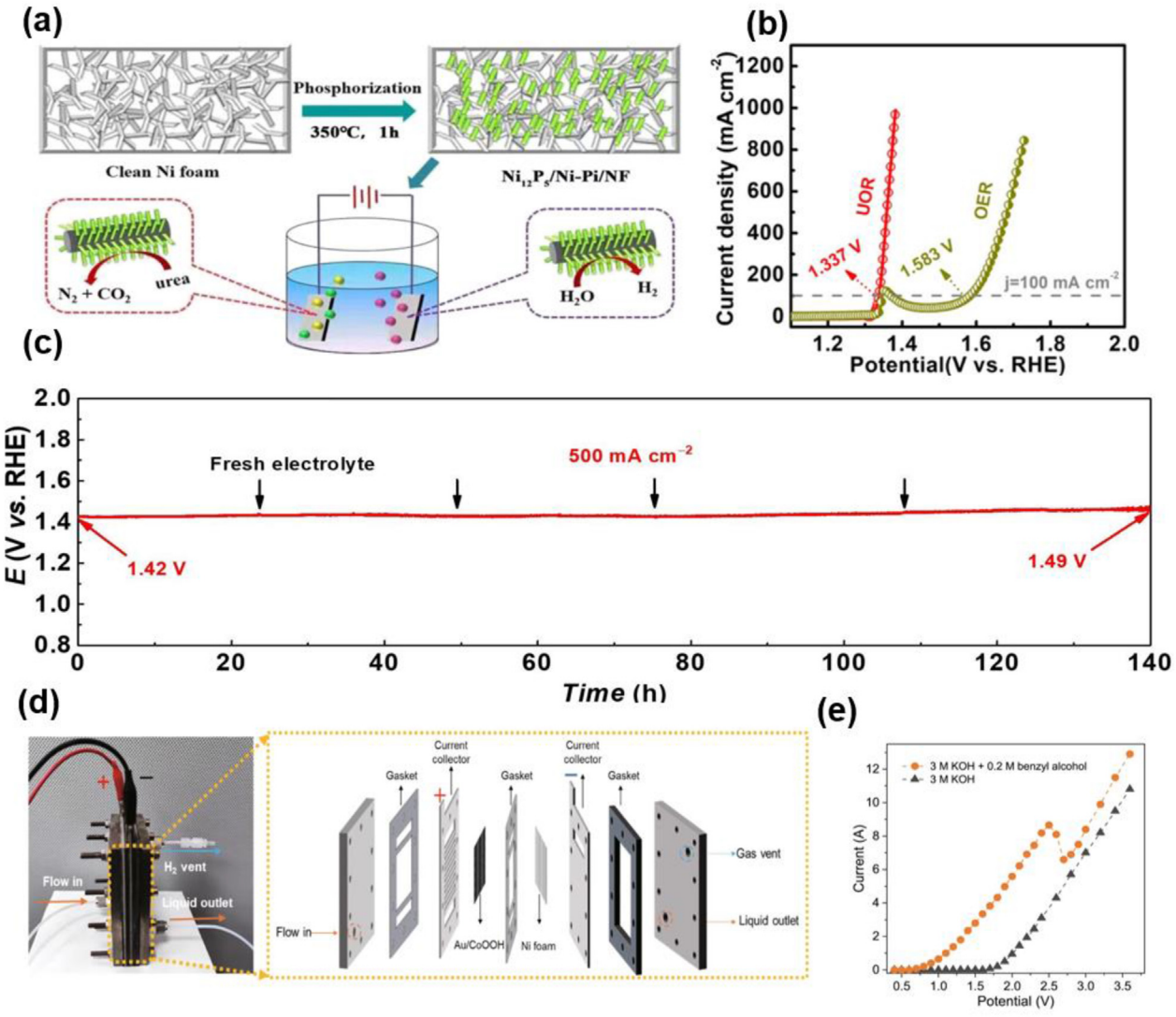

Fig. 5. (a) Synthesis diagram of the formation process the $Ni_{12}P_5$/Ni-Pi/NF electrode, and (b) LSV curves of its in different solutions (Reprinted with permission from Ref. [86] Copyright (2020) ACS.). (c) The stability test of Ni–Co_2VO_4/NF (Reprinted with permission from Ref. [87] Copyright (2022) Elsevier.). (d) Membrane-free flow electrolyzer, and (e) LSV curves of its in different solutions (Reprinted with permission from Ref. [97] Copyright (2022) Springer.).

coupling electrolyzer to drive the overall reaction can keep the long-term stability at 500 mA cm^{-2} for 140 h without significant activity reduction (Fig. 5(c)). In addition, some other types of catalysts, such as $MnO_2/MnCo_2O_4$/Ni [88], Ni_xFeN/Ni_3N [89], and $Fe_2P@Ni_xP$/NF [90], also have the outstanding catalytic performance of UOR. Nevertheless, in UOR process, greenhouse gas (CO_2) inevitably is emitted, which harms the environment. In contrast, hydrazine oxidation (HzOR) coupled with HER is an ecofriendly strategy due to that HzOR product is only N_2. Sun and coworkers designed Ni_2P nano-array grown on NF (Ni_2P/NF) as a fabulous catalyst for HzOR and HER [91]. It was used to assemble a two-electrode electrolytic system, only 1.0 V cell voltage is required at the current density of 500 mA cm^{-2}, and it also has superior long-term stability. Yin et al. [92] constructed the catalyst of $FeWO_4$-WO_3 heterostructure grown on NF, namely $FeWO_4$-WO_3/NF, by hydrothermal reaction and calcination method. The catalyst showed outstanding catalytic activity for HzOR, and its potential was 0.164 V when the current density was as high as 1000 mA cm^{-2}.

As mentioned above, using nitrogen-containing molecular oxidation reaction instead of OER can significantly reduce overpotential at high current density. But in fact, it is very difficult for nitrogen fixation, which inevitably increases the cost of the whole reaction. Compared with this, various alcohols (methanol, ethanol, glycerin, etc.) with low prices and abundant reserves are more practical as ideal substrate molecules to participate in anodic oxidation. As a basic organic molecule, methanol is the simplest saturated monohydric alcohol, which has considerable productivity and is easy to store and transport [93]. Its oxidation products (mainly formic acid) can be directly used as rubber additives, preservatives, disinfection, etc. [94]. However, methanol molecules with high reactivity are easily oxidized to CO_2 under large current,

which limits the efficiency of selective production of value-added products. Fu and coworkers realized the in-situ growth of NiSe hollow nanocrystals on carbon nanotubes by the one-pot method [95]. The obtained material (h-NiSe/CNTs) has a highly cross-linked heterostructure 3D network, which can facilitate mass/charge diffusion. It is proved to be an efficient electrocatalyst suitable for methanol oxidation reaction (MOR), which required only 1.65 V to reach 400 mA cm^{-2} in 1.0 mol L^{-1} KOH with 1.0 mol L^{-1} methanol solution. When the MOR is coupled with HER, compared with electrolyzed water, the power consumption is significantly reduced, and the generation of H_2 is effectively promoted. In a balanced surface state, Ni–OOH species and SeO_x species can synergistically adjust the d band center, which is beneficial to the adsorption of intermediates, and can further inhibit the generation of CO_2, thus making the selective conversion of methanol to value-added formate more favorable. In another work, Fu and co-workers equipped the Ni_3S_2 nanocrystalline grown on carbon nanofibers (Ni_3S_2-CNFs/CC) on the cathode and anode [96]. As for OER, Ni_3S_2-CNFs/CC exhibited better performance than commercial IrO_2. In detail, a potential of 2.04 and 2.13 V was needed to deliver high current densities of 800 and 1000 mA cm^{-2}, respectively. As for MOR, Ni_3S_2-CNFs/CC only needed a potential of 1.67 and 1.74 V to provide 800 and 1000 mA cm^{-2}, respectively. The authors compared the energy consumption of overall water electrolysis with that of HER assisted by methanol. It is found that under the high current density of 600 mA cm^{-2}, it takes about 374.4 J for water electrolysis to generate 1 mmol H_2, while under the same current density, only needs about 308.8 J to generate the same amount of H_2 in methanol-assisted HER electrolyzer. All the results show that Ni_3S_2-CNFs electrocatalyst can efficiently convert methanol to formate at high current density and can assist the cathode to produce hydrogen with extremely low energy consumption. Recently, Duan et al. [97] constructed an Au/MOOHs (M = Co, Ni, Fe) catalyst, using Au as the adsorption site of alcohol molecules and MOOHs as the donor site of OH* to realize the electrocatalytic oxidation of alcohol coupled with cathode hydrogen production at high current densities (potential of 1.5 V to reach 540 mA cm^{-2}). Furthermore, an intermittent voltage input strategy was developed, which reduced AuO_x ($AuO_x \rightarrow Au$) by using the self-reducibility of benzyl alcohol under open-circuit voltage, and realized the continuous reaction of Au/CoOOH catalyst at 250−400 mA cm^{-2} for 24 h and 100−170 mA cm^{-2} for 108 h. Compared with the conventional constant potential strategy, the oxidation rate of benzyl alcohol and hydrogen production rate in this strategy increased by 10 times and 9 times, respectively. To prove the effectiveness of this strategy in practical industrial conditions, the performance of the Au/CoOOH catalyst was further evaluated in a diaphragm-free flow electrolyzer, and the absolute current value was as high as 4.8 A at 2.0 V cell voltage (Fig. 5 (d) and (e)). Recently, biomass or biomass-derived intermediates as a renewable green organic carbon source are also favored by researchers. The 5-hydroxymethylfurfural (HMF) obtained by acid-catalyzed dehydration of C6 carbohydrates is regarded as one of the most commonly used biomass-based furan compounds [98]. Wang's group has designed a Co-doped Ni_3S_2 supported on NF, showing outstanding HMF electrooxidation activity with overpotentials of nearly 1.45 V at the current densities of 497 mA cm^{-2} [99]. Furthermore, when combined with cathode HER in an alkaline medium, the yield of 2,5-furandicarboxylic acid is 330.4 μmol cm^{-2} h^{-1}, and the yield of H_2 is 1000 μmol cm^{-2} h^{-1}.

In particular, electrocatalysis organic synthesis has attracted much attention in recent years. It is an interdisciplinary subject that studies the interaction between organic molecules or catalysts and organic molecules by electrochemical means, which can effectively reduce the activation energy of the reaction and accelerate the conversion of organic substances [100]. Compared with traditional organic reactions, it has the advantages of high efficiency, green, and sustainability. Zhang's group [101] constructed an electrocatalytic reaction system with the three-phase interface, and based on the electrochemically deposited Cu dendrites catalyst, the acetylene impurity concentration in crude ethylene was greatly removed from 1×10^4 ppm to 4 ppm at the space velocity of 9.6×10^4 mL g_{cat}^{-1} h^{-1}, thus realizing the continuous production of polymer-grade ethylene. Compared with the thermocatalytic process, this system was carried out at normal temperature and pressure, with water as a hydrogen source, which effectively reduces the production cost. Recently, Zhang and Wang et al. [102] reported a layered LDH-derived Cu catalyst for an electrochemical acetylene reduction system. In the simulated gas feed, the system provided an acetylene conversion rate of more than 99.9% at the flow rate of 50 mL min^{-1} in the simulated gas feed, resulting in high purity ethylene with ethylene/acetylene volume ratio exceeding 105 and negligible residual hydrogen (0.08 vol.%). This electrochemical technology has potential advantages in replacing traditional solvothermal strategies to realize the conversion of acetylene to ethylene. Compared with other electrochemical reactions, electrocatalytic organic chemistry is still a long way from industrial application, but with the continuous progress of science, this field will make further leaps in the future.

3.3. Electrocatalytic oxygen reduction reaction

Oxygen reduction reaction (ORR) is a multi-electrons transfer process that can be divided into O_2 reduced to H_2O through $4e^-$ pathway, or generated to H_2O_2 through $2e^-$ pathway, which is determined by the adsorption mode, activation and cracking barrier of the catalyst [103,104]. Among them, electrochemical $4e^-$ ORR is an important cathode reaction in fuel cells, which plays a decisive role in the overall efficiency of fuel cells [105]. Proton exchange membrane fuel cell (PEMFC) is the most common type of fuel cell. It is an energy conversion device that uses a proton exchange membrane as an electrolyte to directly convert the chemical energy of externally supplied fuel and oxidant in the air into electric energy, heat energy, and other reaction products through an electrochemical reaction [106]. Compared with traditional energy conversion equipment, it has a series of advantages

including shorter start-up time, lower operating temperature, and high energy density, which is of great significance for alleviating environmental pollution and energy crisis [107,108]. A variety of catalysts (mainly Pt-based materials) have been developed and applied in PEMFC, showing the promising prospect in industrialization application. Zhou and Shao et al. [109] synthesized a catalyst of Pt/perovskite-carbon joint substrate composite. Using composite catalyst at the cathode of PEMFC, a superior power density of 1.14 W cm^{-2}, and a stable running time of >24 h under high current density were achieved. In a recent study, Wu's group designed a series of ultra-small Pt-based intermetallic (Pt_3Co, PtCo, and Pt_3Ti)–Pt skin core–shell catalysts [110]. Among them, Pt–Co intermetallic compound (sub-Pt_3Co-MC) as cathodic catalyst assembled PEMFC showed a high power density of 530 mA cm^{-2}, which was much higher than that of commercial Pt–C catalysts. Despite of the great progress, the cost and durability of the developed catalysts are still obstacles for the full commercialization of PEMFC. Therefore, besides from the development of lower-cost and higher-performance catalysts, it is another feasible approach for the large-scale application of PEMFC that reduces the use of noble metal-based catalysts for effective cost containment and enhancing stability through overall system design and assembling.

As a green oxidant, hydrogen peroxide (H_2O_2) is widely used in wastewater treatment, pulp bleaching, and medical disinfection [111]. The production of H_2O_2 is realized by the anthraquinone process in the traditional industry, whereas it will cause explosive danger during the transportation of H_2O_2 [112]. Electrochemical $2e^-$ ORR at cathodes provides an attractive route to produce H_2O_2, which is more energy-efficient, green, and environment-friendly. The reaction equations of the $2e^-$ ORR in alkaline and acidic conditions can be described by the following: [113].

$$\text{Alkaline}: O_2 + H_2O + 2e^- \rightarrow HO_2^- + OH^- \quad (17)$$

$$\text{Acidic}: O_2 + 2H^+ + 2e^- \rightarrow 2H_2O_2 \quad (18)$$

In order to satisfy the industrial-scale production of H_2O_2, researchers are committed to developing a suitable $2e^-$ ORR catalyst to ensure that its selectivity and activity will not decrease at high current density. Carbon-based catalysts have a broad prospect in the field of $2e^-$ ORR because of their cost-effectiveness and easy adjustment [114]. Recently, a super-hydrophobic three-phase (gas-liquid-solid) N-doped carbon nano polyhedra (NPC) has been designed by Quan's group [115]. Due to its super aerophilic characteristics, NPC can quickly transport and capture O_2 at high current density, which achieves a outstanding H_2O_2 yield rate of 1850.3–7718.4 mmol h^{-1} g_{cat}^{-1} and 83–99% Faraday efficiency (FE) at 50–250 mA cm^{-2} current densities (in 0.1 mol L^{-1} KOH) (Fig. 6 (a)). Zhang et al. [116] designed and synthesized a vertically grown graphene array on carbon paper (VG array) and applied it to H_2O_2 production. In a three-phase flow cell, the maximum FE (H_2O_2) of VG array electrode can achieve 81% when the current density is 200 mA cm^{-2}, and the yield of H_2O_2 can reach 102.8 mg cm^{-2} h^{-1}. The unique graphene array structure can efficiently and quickly transfer O_2 to fully exposed catalytic sites and participate in the reaction, thus achieving the goal of increasing the $2e^-$ ORR catalytic activity. Although the unique advantage of carbon materials, such as a relatively weak combination with oxygen intermediates, makes them exert remarkable $2e^-$ ORR performance in alkaline solutions (under high current), they still can not keep high activity and stability in strongly acidic solutions. The main reason for this phenomenon is that under the negative potential in the acid, the surface area of the catalyst is accumulated with concentrated protons, which easily further reduce the locally produced H_2O_2 molecules to H_2O. In response to this question, Wang et al. [117] have found that the interface of ORR can be adjusted by adding trace metal ions in strongly acidic solutions, which greatly improved the yield of H_2O_2 of commercial carbon black catalysts. By using only 0.01 mol L^{-1} Na_2SO_4 as the cation source, 83% FE (H_2O_2) under industrial-relevant current density (400 mA cm^{-2}) was achieved, which was 25 times higher than that of acidic solution without Na^+. To realize the continuous production of H_2O_2, they further constructed a double-PEM-based solid electrolyte reactor (Fig. 6 (b)). With only 0.03 mol L^{-1} Na_2SO_4 as the cation source, the 90% FE (H_2O_2) and excellent stability were achieved. In view of the above performance, it is expected to continuously conduct $2e^-$ ORR to obtain H_2O_2 by renewable power in commercial applications. Another promising candidate catalyst is single-atom catalysts, which has unique electronic-geometric structure and high atom utilization. Representatively, using the straightforward strategy, Li et al. [118] have constructed Ni single-atom catalyst supported on carboxyl functionalized multiwalled carbon nanotubes (N_4–Ni_1–O_2/OCNTs), which has a super-six-coordination structure. This catalyst shows an outstanding H_2O_2 production rate, up to 5.7 mmol cm^{-2} h^{-1}. In large current densities of 200 mA cm^{-2}, a promoted FE (H_2O_2) (~96%) was achieved.

3.4. Electrocatalytic CO_2 conversion

Electrocatalytic conversion of CO_2 at commercially relevant current densities can not only reduce CO_2 concentration in the atmosphere but also use CO_2 as chemical raw materials to produce value-added chemicals [119]. According to the number of carbon atoms in CO_2 conversion products, it can be divided into C_1 and C_{2+} products [120]. Among them, C_1 products are relatively simple and easy to obtain, mainly because of their shorter reaction steps and fast kinetics. Firstly, the reduction of CO_2 to *COOH by cooperative protons and electrons transfer. Then, other protons and electrons attack OH in *COOH to generate *CO and H_2O. Finally, *CO is desorbed from the electrode surface to obtain CO. Feng and coworkers designed and fabricated a catalyst of the Ni single atom immobilized on N-doped carbon support (Ni–N–C) for CO_2 conversion [121]. Remarkably, as shown in Fig. 7(a), the Ni–N–C has excellent CO_2 to CO electrolysis performance and achieves 90.8% FE at the high current density of 726 mA cm^{-2} in an industrial flow cell. DFT calculation confirmed that with the increase of thermal activation

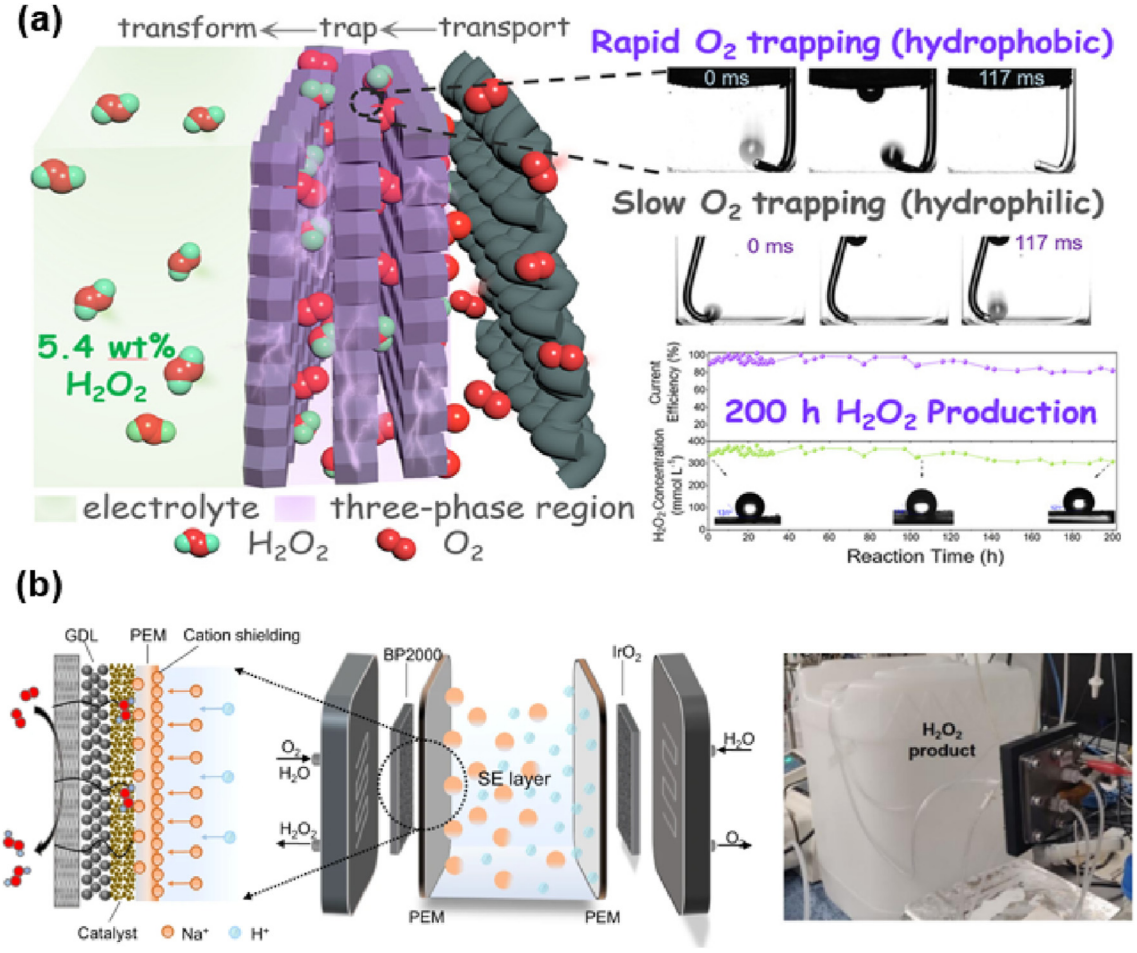

Fig. 6. (a) The NPC nano polyhedra for H_2O_2 production (Reprinted with permission from Ref. [115] Copyright (2021) ACS.). (b) Schematic illustration of reducing O_2 to H_2O_2 in the SE cell with double-PEM configuration (Reprinted with permission from Ref. [117] Copyright (2022) Springer.).

temperature, the shortened Ni–N bond plays an important role in CO_2 conversion. Hu and Zhao et al. [122] have designed a cooperative Ni single atom on nanoparticle (NiSA/NP) by simple direct solid-state pyrolysis. Based on the membrane electrode assembly device, NiSA/NP||NiFe cell delivers can produce CO with a high current density of 308.4 mA cm^{-2} and a maximum FE (CO) of 99% at a cell voltage of −2.3 V. The impressive performance has been proven to be related to the enhanced binding of the intermediate COOH* on the electron enrichment of single Ni sites. Recently, Chen and Wu et al. [123] have explored a Co–Cu diatomic site catalyst (CoCu-DASC) via a facile pyrolysis approach, which achieved significant activity on CO_2 conversion with FE (CO) as high as 99% (Fig. 7(b)), and a high CO partial current density of 483 mA cm^{-2} was obtained (Fig. 7(c)). Compared with the production of C_1 products, it seems more difficult to deeply reduce CO_2 to C_{2+} products, mainly because this process is a complex multi-step reaction. To date, Cu-based materials have been considered the component catalyst that can reduce CO_2 to C_{2+} products with considerable efficiency. This particularity has aroused the interest of many researchers, and various modification methods have been proposed. Zhang et al. [124] used the hydrothermal method to synthesize a fluorine-modified Cu catalyst, which exhibited notable CO_2 reduction activity with a C_{2+} (mainly C_2H_4 and CH_3CH_2OH) FE of 80% at ultrahigh density (up to 1.6 A cm^{-2}), and the production rate of C_{2+} is about 4013 μmol h^{-1} cm^{-2}. Duan et al. [125] have fabricated different heteroatom (N, P, S, O) engineered Cu-based compounds with a facile hydrothermal reaction, among which N-modified Cu catalyst exhibits remarkable FE (C_{2+}) of over 70% under 1100 mA cm^{-2}. Sun et al. [126] innovatively modified an anti-swelling anion-exchange ionomer (AEI) on the surface of a Cu-based catalyst (AEI-OD-Cu), and achieved the purpose of producing C_{2+} products with outstanding selectivity under high current density through regulation of the local environment (Fig. 7(d)). Introducing AEI modified electrocatalyst possessed the following advantages: (i) the designed AEI has quaternary ammonium groups ($-N(CH_3)_3^+$), which can generate electrostatic interaction with OH^- in the electrolyte, thus increasing the alkalinity of the local surface of the catalyst. (ii) the unique structure of AEI can inhibit HER by controlling the water content in the catalyst layer, so that COCO* is easier to be further hydrogenated, thus helping to improve the selectivity and activity of CO_2 to C_{2+}; (iii) the $-N(CH_3)_3^+$group on AEI plays an important role in CO_2 capture. Relying on the above characteristics, the

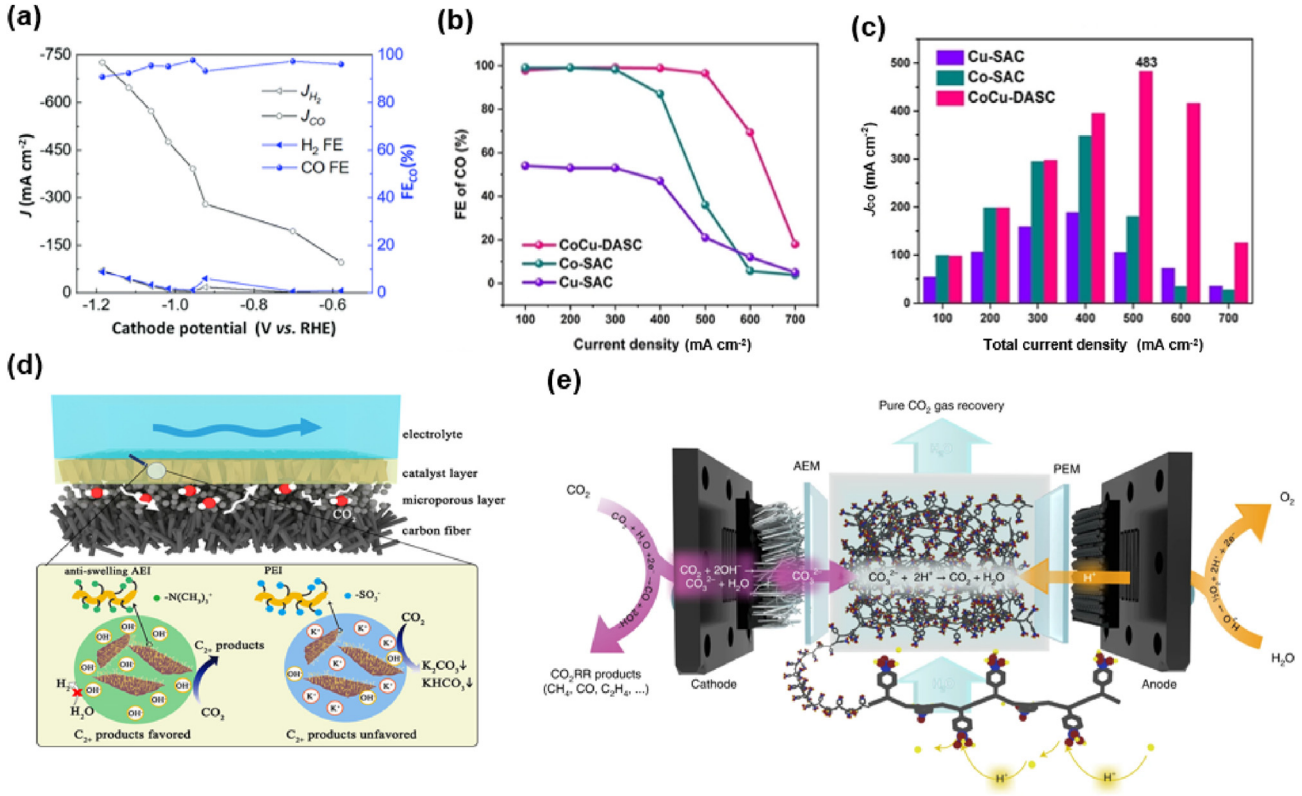

Fig. 7. (a) Flow cell electrolyze performance of the Ni–N–C (Reprinted with permission from Ref. [121] Copyright (2022) Royal Society of Chemistry.). (b) The Faradaic efficiencies of CO and (c) CO partial current density in flow cell (Reprinted with permission from Ref. [123] Copyright (2022) Wiley.). (d) Manipulation of CO_2 to C_{2+} activity and selectivity through local environment construction (Reprinted with permission from Ref. [126] Copyright (2022) ACS.). (e) PSE reactor design for crossover CO_2 recovery (Reprinted with permission from Ref. [127] Copyright (2022) Springer.).

obtained AEI-OD-Cu catalyst can reduce CO_2 to C_{2+} (C_2H_4, C_2H_5OH, C_3H_7OH) with 85.1% FE at 800 mA cm^{-2}, showing promise for industrial CO_2RR applications. Wang et al. [127] designed a porous solid electrolyte (PSE) reactor to successfully recover lost CO_2 gas during CO_2 reduction electrolysis while maintaining high catalytic performances (Fig. 7(e)). This strategy avoids using extra gas separation equipment or energy required to separate crossover CO_2 from impurities (especially oxygen). At present, great progress has been made in electrocatalytic CO_2 conversion under high currents, but to further realize its complete industrialization, it is necessary to study the factors affecting the reaction conditions such as pH, potential dependence, and electrolyte effect.

4. Large-scale integrated processes for holistic renewable energy production and utilization

We have demonstrated many potential industrial photo/electrocatalytic processes for energy and environmental application in this review. Among them, hydrogen generation is one of the most attractive approaches because hydrogen is a zero-emission energy vector that only produces water when used. Besides, hydrogen can couple with other renewable photo/electrocatalytic processes and plays a major role in developing new strategies for converting industrial CO_2 emissions into important platform chemicals [128]. However, when it comes to direct hydrogen utilization, long-distance transportation and storage of large quantities of hydrogen are a great challenge due to its low volumetric energy density (2.97 Wh L^{-1}; H_2 gas, 273 K, 1 atm), which would result in a massively cost and pose serious safety concerns. Recently, the decomposition of liquid hydrogen carriers to produce hydrogen has emerged as an alternative hydrogen handling technique to accelerate the development of the hydrogen economy. For example, NH_3 has been regarded as a promising medium for promoting energy transition toward hydrogen due to its high gravimetric hydrogen content (17.7 wt%) and can be easily liquefied under c.a. 8 atm pressure at room temperature. Moreover, NH_3 production, storage, and distribution have a well-established industrial infrastructure compared to the direct hydrogen handling system [129].

To date, industries have begun to launch large-scale green ammonia production projects using the hydrogen supply from water electrolysis without needing a major change in the conventional Haber-Bosch NH_3 synthesis reactor configuration [130,131]. The combined technologies and integrated catalytic systems are often implemented to realize holistic green energy production and utilization. For example, in collaboration with Siemens, Tsang's research group set up a power-to-ammonia demonstrator, which can give 11 tonnes p.a. green ammonia from a 13 kW wind turbine using a proton exchange membrane water electrolyzer to produce H_2 in

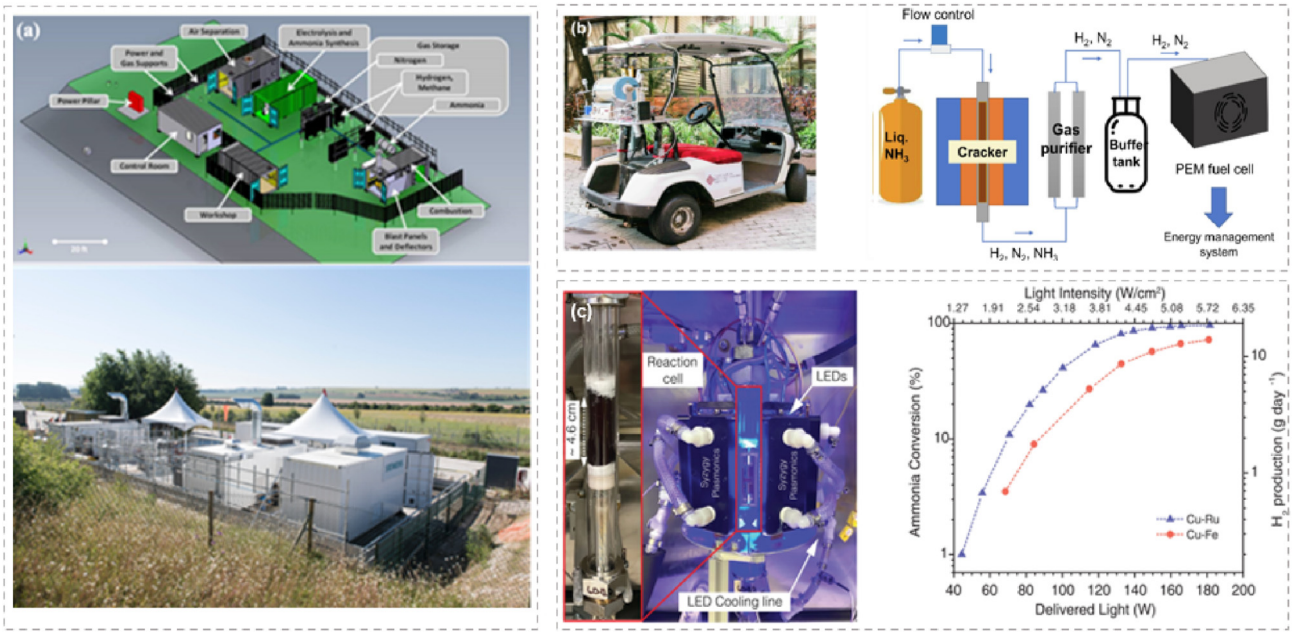

Fig. 8. (a) Siemens Green Ammonia Demonstrator site layout (top) and onsite photograph (bottom) [132]. (b) Photograph of the ammonia-powered fuel cell golf cart (left) and an overview of the powerpack system (right) (Reprinted with permission from Ref. [136] Copyright (2023) Elsevier.). (c) Photograph of the reaction cell of plasmonic photocatalysts for hydrogen production from ammonia (Reprinted with permission from Ref. [137] Copyright (2022) American Association for the Advancement of Science.).

combination with N_2 from air separation over Fe-based catalyst (Fig. 8(a)) [132]. In addition, multiple renewable power sources (wind, solar, tidal, etc.) can be adopted to power up the photo/electrolytic hydrogen production to ensure sufficient green hydrogen generation for the remote or off-shore ammonia production plants [129]. Besides the traditional thermal NH_3 synthesis, photocatalytic and photo-electrocatalytic synthesis are two novel methods to generate green ammonia and have received incredible attention in the research community. However, the direct photo/electro reduction of nitrogen to ammonia production still lacks stability, economic feasibility, and catalytic activity.

NH_3 decomposition is considered a practical approach that generates nitrogen and hydrogen gas mixture via the catalytic process. The produced hydrogen can be used directly as fuel to power fuel cell systems to generate electricity, or as hydrogen supply for other processes like powering, heating, and feedstock in chemical reactions [133–135]. For example, an NH_3-powered fuel cell electric system was developed by Li and coworkers [136]. The integration of NH_3 supply, decomposition reactor, gas purifier, fuel cell, and energy management system formed a successful powertrain that thrusts a golf cart into motion (Fig. 8(b)). However, the current challenge is that hydrogen production from NH_3 often requires high-temperature conditions. Therefore, developing highly efficient catalysts for ammonia decomposition under mild conditions through novel processes and new reactor designs is urgently required. Very recently, Yuan et al. [137] developed a scalable Cu–Fe-catalyst for plasmonic photocatalysis and used light sources, such as sunlight or energy-efficient LEDs, to transform NH_3 into hydrogen, which may be competitive with thermal catalysts used in this hydrogen carrier system (Fig. 8(c)).

Overall, green energy is becoming significant in our everyday life. To realize clean energy at a large scale, continuous investments in developing and investigating renewable energy are required from different research areas, particularly by combining conventional technologies with advanced photo/electro techniques from multiple disciplines to deliver a practical energy solution.

5. Conclusions and perspectives

In recent years, the industrial application of photo/electrocatalysis has always been a field of interest to researchers and has undergone rapid development. Given the important role of photo/electrocatalysis in solving future energy and environmental problems, this review introduces the progress of photo/electrocatalysis industrialization.

Photocatalytic applications mainly focus on the following aspects: photocatalytic solar hydrogen production, pollutant treatment and conversion of CO_2. At present, some progress has been made in large-scale applications, but the problem of cost and efficiency is still the bottleneck restricting its further development. With regard to the commercialization prospect of electrocatalysis, we have classified the recently most reported electrocatalytic reactions into four categories (water splitting, electrocatalytic conversion of organic molecules, oxygen reduction reaction, and electrocatalytic CO_2 conversion) by using representative catalysts, and introduced their catalytic effect and potential conversion rate under industrial current. At the same time, considering that high current

density usually damages the catalyst, the stability of the catalyst system was also investigated. Progress has clearly been made in the industrial application of photo/electrocatalysis; however, from the perspective of both scientific and technological, there are still exist many challenges, thus should lead the direction of future research.

It has been proved that the surface of photo/electrocatalysts will change dramatically under industrial conditions, which will further greatly affect the catalytic performance in continuous operation, thus making the reaction kinetics different from that in the laboratory scale. In consequence, the preparation of self-supporting catalysts should be considered first when designing catalysts and the reaction mechanism needs to be further explored. Considering that the morphology, composition, valence state of photo/electrocatalysis, and the local environment around the active substance are changing dynamically under different experimental conditions, it will definitely hinder the accurate identification and exploration of the active substance/site, crystal plane, and structure. Therefore, it is necessary to use some advanced in situ/operando characterization techniques to clarify the real active sites and determine the catalytic mechanism. Besides focusing on the construction of high-performance catalysts, several emerging reactions with large-scale application prospects certainly deserve special attention, such as converting nitrogen in the air into ammonia by photo-/photoelectric/photothermal catalytic reaction systems to provide nitrogen fertilizer for agricultural plant growth and development. Compared with the current industrial mature synthetic ammonia process (Haber-Bosch process), this technology takes place in milder temperature conditions, which is energy-efficient and ecologically friendly. It is also very important to design the whole coupling system and its device. Such as coupling photo/electrocatalytic hydrogen production with other reaction systems, including reduction of CO_2, selective oxidation of organics, and oxidative degradation of contaminants. Choosing the appropriate reaction for coupling can reduce energy consumption, increase the added value of products, or speed up the reaction rate so that the practicability of the catalytic system can be improved.

In summary, in order to speed up the industrial application of photo/electrocatalysis, it is necessary to further explore the reaction mechanism, and design new reaction systems and devices in the future. This review is expected to provide enlightenment for the industrial application of photo/electrocatalysis.

Conflict of interest

The authors declare that they have no known competing financial interests or personal relationships that could have appeared to influence the work reported in this paper.

Acknowledgments

This research was supported by the National Natural Science Foundation of China (22278030, 22090032, 22090030, 22288102, 22242019), the Fundamental Research Funds for the Central Universities (buctrc202119, 2312018RC07), Major Program of Qingyuan Innovation Laboratory (Grant No. 001220005) and the Experiments for Space Exploration Program and the Qian Xuesen Laboratory, China Academy of Space Technology.

References

[1] X. Fan, W. Sun, F. Meng, A. Xing, J. Liu, Green Energy Environ. 3 (2018) 2–19.
[2] A. Remmel, S. Ratso, G. Divitini, M. Danilson, V. Mikli, M. Uibu, J. Aruväli, I. Kruusenberg, ACS Sustain. Chem. Eng. 10 (2022) 134–145.
[3] M. Ferri, L. Delafontaine, S. Guo, T. Asset, P. Cristiani, S. Campisi, A. Gervasini, P. Atanassov, ACS Energy Lett. 7 (2022) 2304–2310.
[4] Z. Wu, J. Mei, Q. Liu, S. Wang, W. Li, S. Xing, J. Bai, J. Yang, W. Luo, O. Guselnikova, A.P. O'Mullane, Y. Gu, Y. Yamauchi, T. Liao, Z. Sun, J. Mater. Chem. A 10 (2022) 808–817.
[5] N. Ali, T.T. Tsega, Y. Cao, S. Abbas, W. Li, A. Lqbal, H. Fazal, Z. Xin, J. Zai, X. Qian, Nano Res. 14 (2021) 3358–3364.
[6] Y. Wu, X. Chen, J. Cao, Y. Zhu, W. Yuan, Z. Hu, Z. Ao, G. Brudvig, F. Tian, J. Yu, C. Li, Appl. Catal. B Environ. 303 (2022) 120878.
[7] L. Zhang, R. Li, H. Zang, H. Tan, Z. Kang, Y. Wang, Y. Li, Energy Environ. Sci. 14 (2021) 6191–6210.
[8] D.C. Nguyen, T.L.L. Doan, S. Prabhakaran, D.T. Tran, D.H. Kim, J.H. Lee, N.H. Kim, Nano Energy 82 (2021) 105750.
[9] Y. Chen, Z. Fan, J. Wang, C. Ling, W. Niu, Z. Huang, G. Liu, B. Chen, Z. Lai, X. Liu, B. Li, Y. Zong, L. Gu, J. Wang, X. Wang, H. Zhang, J. Am. Chem. Soc. 142 (2020) 12760–12766.
[10] N. Kim, J.S. Nam, J. Jo, J. Seong, H. Kim, Y. Kwon, M.S. Lah, J.H. Lee, T.H. Kwon, J. Ryu, Nanoscale Horiz. 6 (2021) 379–385.
[11] N. Kumar, K. Naveen, M. Kumar, T.C. Nagaiah, R. Sakla, A. Ghosh, V. Siruguri, S. Sadhukhan, S. Kanungo, A.K. Paul, ACS Appl. Energy Mater. 4 (2021) 1323–1334.
[12] J. Luo, M. Wang, L. Chen, J. Shi, J. Energy Chem. 66 (2022) 52–60.
[13] Y. Yang, C. Zhou, W. Wang, W. Xiong, G. Zeng, D. Huang, C. Zhang, B. Song, W. Xue, X. Li, Z. Wang, D. He, H. Luo, Z. Quyang, Chem. Eng. J. 405 (2021) 126547.
[14] N.R.A.M. Shah, R.M. Yunus, N.N. Rosman, W.Y. Wong, K. Arifin, L.J. Minggu, Int. J. Hydrogen Energy 46 (2021) 9324–9340.
[15] G. Huang, W. Ye, C. Lv, D.S. Butenko, C. Yang, G. Zhang, P. Lu, Y. Xu, S. Zhang, H. Wang, Y. Zhu, D. Yang, J. Mater. Sci. Technol. 108 (2022) 18–25.
[16] Y. Ying, Z. Lin, H. Huang, ACS Energy Lett. 8 (2023) 1416–1423.
[17] L. An, C. Wei, M. Lu, H. Liu, Y. Chen, G.G. Scherer, A.C. Fisher, P. Xi, Z.J. Xu, C. Yan, Adv. Mater. 33 (2021) 2006328.
[18] J.P. Hughes, J. Clipsham, H. Chavushoglu, S.J. Rowley-Neale, C.E. Banks, Renew. Sust. Energ. Rev. 139 (2021) 110709.
[19] Y. Zhang, C. Han, J. Gao, L. Pan, J. Wu, X. Zhu, J. Zou, ACS Catal. 11 (2021) 12485–12509.
[20] J. Song, C. Wei, Z. Huang, C. Liu, L. Zeng, X. Wang, Z.J. Xu, Chem. Soc. Rev. 49 (2020) 2196–2214.
[21] Y. Yan, P. Wang, J. Lin, J. Cao, J. Qi, J. Energy Chem. 58 (2021) 446–462.
[22] T. Wu, C. Dong, D. Sun, F. Huang, Nanoscale 13 (2021) 1581–1595.
[23] Z. Xiao, C. Xie, Y. Wang, R. Chen, S. Wang, J. Energy Chem. 53 (2021) 208–225.
[24] Y. Zhao, Y. Lu, L. Chen, X. Wei, J. Zhu, Y. Zheng, ACS Appl. Mater. Interfaces 12 (2020) 46073–46083.
[25] G. Zhao, Y. Jiang, S. Dou, W. Sun, H. Pan, Sci. Bull. 66 (2021) 85–96.
[26] R. Kumar, P. Raizada, N. Verma, A. Hosseini-Bandegharaei, V.K. Thakur, Q. Van Le, V.H. Nguyen, R. Selvasembian, P. Singh, J. Clean. Prod. 297 (2021) 126617.
[27] C. Hu, R. Paul, Q. Dai, L. Dai, Chem. Soc. Rev. 50 (2021) 11785–11843.
[28] Y. Qian, F. Zhang, H. Pang, Adv. Funct. Mater. 31 (2021) 2104231.

[29] T. Lai, J. Wang, W. Xiong, H. Wang, M. Yang, T. Li, X. Kong, X. Zou, Y. Zhao, D. O'Hare, Y.-F. Song, Chem. Eng. Sci. 257 (2022) 117704.
[30] A. Fujishima, K. Honda, Nature 238 (1972) 37–38.
[31] G. Liao, Y. Gong, L. Zhang, H. Gao, G. Yang, B. Fang, Energy Environ. Sci. 12 (2019) 2080–2147.
[32] S. Han, Q. Yun, S. Tu, L. Zhu, W. Cao, Q. Lu, J. Mater. Chem. A 7 (2019) 24691–24714.
[33] Y. Peng, X. Guo, S. Xu, Y. Guo, D. Zhang, M. Wang, G. Wei, X. Yang, Z. Li, Y. Zhang, F. Tian, J. Energy Chem. 75 (2022) 276–284.
[34] W. Li, X. Chu, F. Wang, Y. Dang, X. Liu, T. Ma, J. Li, C. Wang, Appl. Catal. B Environ. 304 (2022) 121000.
[35] X. Liu, P. Cheng, X. Zhang, T. Sen, J. Liu, J. Ren, H. Wang, S. Li, W. Liu, J. Mater. Chem. A 9 (2021) 14515–14523.
[36] Y. Goto, T. Hisatomi, Q. Wang, T. Higashi, K. Ishikiriyama, T. Maeda, Y. Sakata, S. Okunaka, H. Tokudome, M. Katayama, S. Akiyama, H. Nishiyama, Y. Inoue, T. Takewaki, T. Setoyama, T. Minegishi, T. Takata, T. Tamada, K. Domen, Joule 2 (2018) 509–520.
[37] H. Nishiyama, T. Yamada, M. Nakabayashi, Y. Maehara, M. Yamaguchi, Y. Kuromiya, Y. Nagatsuma, H. Tokudome, S. Akiyama, T. Watanabe, R. Narushima, S. Okunaka, N. Shibata, T. Takata, T. Hisatomi, K. Domen, Nature 598 (2021) 304–307.
[38] T. Suguro, F. Kishimoto, N. Kariya, T. Fukui, M. Nakabayashi, N. Shibata, T. Takata, K. Domen, K. Takanabe, Nat. Commun. 13 (2022) 5698.
[39] Y. Zhao, C. Ding, J. Zhu, W. Qin, X. Tao, F. Fan, R. Li, C. Li, Angew. Chem. Int. Ed. 59 (2020) 9653–9658.
[40] Y. Dai, C. Li, Y. Shen, T. Lim, J. Xu, Y. Li, H. Niemantsverdriet, F. Besenbacher, N. Lock, R. Su, Nat. Commun. 9 (2018) 60.
[41] C. Huang, J. Qiao, R. Ci, X. Wang, Y. Wang, J. Wang, B. Chen, C. Tung, L. Wu, Chem 7 (2021) 1244–1257.
[42] C. Huang, R. Ci, J. Qiao, X. Wang, K. Feng, B. Chen, C. Tung, L. Wu, Angew. Chem. Int. Ed. 60 (2021) 11779–11783.
[43] L. Andronic, L. Isac, S. Miralles-Cuevas, M. Visa, I. Oller, A. Duta, S. Malato, J. Hazard. Mater. 320 (2016) 469–478.
[44] L. Huang, X. Huang, J. Yan, Y. Liu, H. Jiang, H. Zhang, J. Tang, Q. Liu, J. Hazard. Mater. 442 (2023) 130024.
[45] S. Deepracha, L. Atfane, A. Ayral, M. Ogawa, Sep. Purif. Technol. 262 (2021) 118307.
[46] H. Dai, X. Yuan, L. Jiang, H. Wang, J. Zhang, J. Zhang, T. Xiong, Coord. Chem. Rev. 441 (2021) 213985.
[47] O. Sacco, V. Vaiano, L. Rizzo, D. Sannino, J. Clean. Prod. 175 (2018) 38–49.
[48] W. Zhao, I.W. Chen, F. Huang, Nano Today 27 (2019) 11–27.
[49] O. Baaloudj, A.K. Badawi, H. Kenfoud, Y. Benrighi, R. Hassan, N. Nasrallah, A.A. Assadi, J. Water Process Eng. 48 (2022) 102847.
[50] O. Debono, V. Gaudion, N. Redon, N. Locoge, F. Thevenet, Chem. Eng. J. 353 (2018) 394–409.
[51] P. Huang, Y. Li, Y. Shu, S. Liang, X. Huang, Y. Gan, G. Li, H. Huang, Sci. Total Environ. 857 (2023) 159295.
[52] J. Fu, K. Jiang, X. Qiu, J. Yu, M. Liu, Mater. Today 32 (2020) 222–243.
[53] K. Li, B. Peng, T. Peng, ACS Catal. 6 (2016) 7485–7527.
[54] G. Zhao, J. Hu, X. Long, J. Zou, J. Yu, F. Jiao, Small 17 (2021) 2102155.
[55] C. Shih, T. Zhang, J. Lim C. Bai, Joule 2 (2018) 1925–1949.
[56] V. Andrei, G.M. Ucosk, C. Pornrungroj, C. Uswachoke, Q. Wang, D.S. Achilleos, H. Kasap, K.P. Sokol, R.A. Jagt, H. Lu, T. Lawson, A. Wagner, S.D. Pike, D.S. Wrigh, R.L.Z. Hoye, J.L. MacManus-Driscoll, H.J. Joyce, R.H. Friend, E. Reisner, Nature 608 (2022) 518–522.
[57] S. Zoller, E. Koepf, D. Nizamian, M. Stephan, A. Patané, P. Haueter, M. Romero, J. González-Aguilar, D. Lieftink, E. Wit, S. Brendelberger, A. Sizmann, A. Steinfeld, Joule 6 (2022) 1606–1616.
[58] Y. Zhao, Z. Li, M. Li, J. Liu, X. Liu, G.I.N. Waterhouse, Y. Wang, J. Zhao, W. Gao, Z. Zhang, R. Long, Q. Zhang, L. Gu, X. Liu, X. Wen, D. Ma, L. Wu, C. Tung, T. Zhang, Adv. Mater. 30 (2018) 1803127.
[59] Y. Luo, Z. Zhang, M. Chhowalla, B. Liu, Adv. Mater. 34 (2022) 2108133.
[60] K. Zhang, X. Liang, L. Wang, K. Sun, Y. Wang, Z. Xie, Q. Wu, X. Bai, M.S. Hamdy, H. Chen, X. Zou, Nano Res. Energy 1 (2022) e9120032.
[61] D. Aili, M.R. Kraglund, S.C. Rajappan, D. Serhiichuk, Y. Xia, V. Deimede, J. Kallitsis, C. Bae, P. Jannasch, D. Henkensmeier, J.O. Jensen, ACS Energy Lett. 8 (2023) 1900–1910.
[62] Q. Wu, Y. Wang, K. Zhang, Z. Xie, K. Sun, W. An, X. Liang, X. Zou, Mater. Chem. Front. 7 (2023) 1025–1045.
[63] J. Sun, F. Tian, F. Yu, Z. Yang, B. Yu, S. Chen, Z. Ren, H. Zhou, ACS Catal. 10 (2020) 1511–1519.
[64] Y. Cheng, H. Song, H. Wu, P. Zhang, Z. Tang, S. Lu, Chem. Asian J. 15 (2020) 3123–3134.
[65] M. Jin, X. Zhang, S. Niu, Q. Wang, R. Huang, R. Ling, J. Huang, R. Shi, A. Amini, C. Cheng, ACS Nano 16 (2022) 11577–11597.
[66] J. Joyner, E.F. Oliveira, H. Yamaguchi, K. Kato, S. Vinod, D.S. Galvao, D. Salpekar, S. Roy, U. Martinez, C.S. Tiwary, S. Ozden, P.M. Ajayan, ACS Appl. Mater. Interfaces 12 (2020) 12629–12638.
[67] C. Zhang, Y. Luo, J. Tan, Q. Yu, F. Yang, Z. Zhang, L. Yang, H. Cheng, B. Liu, Nat. Commun. 11 (2020) 3724.
[68] D. Zhang, F. Wang, W. Zhao, M. Cui, X. Fan, R. Liang, Q. Ou, S. Zhang, Adv. Sci. 9 (2022) 2202445.
[69] B. Zhang, L. Zhang, Q. Tan, J. Wang, J. Liu, H. Wan, L. Miao, J. Jiang, Energy Environ. Sci. 13 (2020) 3007–3013.
[70] C. Yang, W. Zhong, K. Shen, Q. Zhang, R. Zhao, H. Xiang, J. Wu, X. Li, N. Yang, Adv. Energy Mater. 12 (2022) 2200077.
[71] Y. Zhou, W. Hu, Y. Zhen, B. Dong, Y. Dong, R. Fan, B. Liu, D. Liu, Y. Chai, Appl. Catal. B Environ. 309 (2022) 121230.
[72] Q. Du, P. Su, Z. Cao, J. Yang, C.A.H. Price, J. Liu, Sus. Mater. Technol. 29 (2021) e00293.
[73] F. Zeng, C. Mebrahtu, L. Liao, A.K. Beine, R. Palkovits, J. Energy Chem. 69 (2022) 301–329.
[74] L. Yang, Z. Liu, S. Zhu, L. Feng, W. Xing, Mater. Today Phys. 16 (2021) 100292.
[75] S. Anantharaj, S. Kundu, S. Noda, Nano Energy 80 (2021) 105514.
[76] X. Li, C. Liu, Z. Fang, L. Xu, C. Lu, W. Hou, Small 18 (2022) 2104354.
[77] H. Chen, J. Li, Y. Shen, W. Jiao, J. Wang, Y. Zou, X. Zou, Appl. Catal. B Environ. 316 (2022) 121605.
[78] Y. Liu, X. Liang, L. Gu, Y. Zhang, G. Li, X. Zou, J. Chen, Nat. Commun. 9 (2018) 2609.
[79] L. Zhang, C. Chang, C. Hsu, C. Chang, S. Lu, J. Mater. Chem. A 5 (2017) 19656–19663.
[80] X. Zhang, J. Li, Y. Yang, S. Zhang, H. Zhu, X. Zhu, H. Xing, Y. Zhang, B. Huang, S. Guo, E. Wang, Adv. Mater. 30 (2018) 1803551.
[81] H. Liu, X. Li, L. Chen, X. Zhu, P. Dong, M.O.L. Chee, M. Ye, Y. Guo, J. Shen, Adv. Funct. Mater. 32 (2022) 2107308.
[82] T. Wu, S. Xu, Z. Zhang, M. Luo, R. Wang, Y. Tang, J. Wang, F. Huang, Adv. Sci. 9 (2022) 2202750.
[83] Z. Wang, G. Qian, T. Yu, J. Chen, F. Shen, L. Luo, Y. Zou, S. Yin, Chem. Eng. J. 434 (2022) 134669.
[84] Y. Wang, X. Li, Z. Huang, H. Wang, Z. Chen, J. Zhang, X. Zheng, Y. Deng, W. Hu, Angew. Chem. Int. Ed. 62 (2023) e202215256.
[85] L. Chen, J. Shi, J. Mater. Chem. A 6 (2018) 13538–13548.
[86] X. Xu, P. Du, T. Guo, B. Zhao, H. Wang, M. Huang, ACS Sustain. Chem. Eng. 8 (2020) 7463–7471.
[87] M. Pan, G. Qian, T. Yu, J. Chen, L. Luo, Y. Zou, S. Yin, Chem. Eng. J. 435 (2022) 134986.
[88] C. Xiao, S. Li, X. Zhang, D.R. MacFarlane, J. Mater. Chem. A 5 (2017) 7825–7832.
[89] F. Cai, L. Liao, Y. Zhao, D. Li, J. Zeng, F. Yu, H. Zhou, J. Mater. Chem. A 9 (2021) 10199–10207.
[90] T. Guo, X. Xu, X. Wang, J. Zhou, H. Wang, Z. Shi, M. Huang, Chem. Eng. J. 417 (2021) 128067.
[91] C. Tang, R. Zhang, W. Lu, Z. Wang, D. Liu, S. Hao, G. Du, A.M. Asiri, X. Sun, Angew. Chem. Int. Ed. 56 (2017) 842–846.
[92] F. Shen, Z. Wang, Y. Wang, G. Qian, M. Pan, L. Luo, G. Chen, H. Wei, S. Yin, Nano Res. 14 (2021) 4356–4361.
[93] X. Wei, S. Wang, Z. Hua, L. Chen, J. Shi, ACS Appl. Mater. Interfaces 10 (2018) 25422–25428.

[94] X. Wei, Y. Li, L. Chen, J. Shi, Angew. Chem. Int. Ed. 60 (2021) 3148–3155.
[95] B. Zhao, J. Liu, C. Xu, R. Feng, P. Sui, L. Wang, J. Zhang, J. Luo, X. Fu, Adv. Funct. Mater. 31 (2021) 2008812.
[96] B. Zhao, J. Liu, X. Wang, C. Xu, P. Sui, R. Feng, L. Wang, J. Zhang, J. Luo, X. Fu, Nano Energy 80 (2021) 105530.
[97] Z. Li, Y. Yan, S. Xu, H. Zhou, M. Xu, L. Ma, M. Shao, X. Kong, B. Wang, L. Zheng, H. Duan, Nat. Commun. 13 (2022) 147.
[98] Y. Yang, T. Mu, Green Chem. 23 (2021) 4228–4254.
[99] Y. Sun, J. Wang, Y. Qi, W. Li, C. Wang, Adv. Sci. 9 (2022) 2200957.
[100] C. Zhu, N.W.J. Ang, T.H. Meyer, Y. Qiu, L. Ackermann, ACS Cent. Sci. 7 (2021) 415–431.
[101] J. Bu, Z. Liu, W. Ma, L. Zhang, T. Wang, H. Zhang, Q. Zhang, X. Feng, J. Zhang, Nat. Catal. 4 (2021) 557–564.
[102] R. Shi, Z. Wang, Y. Zhao, G.I.N. Waterhouse, Z. Li, B. Zhang, Z. Sun, C. Xia, H. Wang, T. Zhang, Nat. Catal. 4 (2021) 565–574.
[103] C. Zhou, S. Zhao, H. Meng, Y. Han, Q. Jiang, B. Wang, X. Shi, W. Zhang, L. Zhang, R. Zhang, Nano Lett. 21 (2021) 9633-9461.
[104] X. Huang, M. Song, J. Zhang, J. Zhang, W. Liu, C. Zhang, W. Zhang, D. Wang, Nano Res. 15 (2022) 3927–3932.
[105] W. Jiang, Y. Li, Y. Xu, T. Jiang, M. Zhao, M. Deng, R. Wu, Y. Wang, Chem. Eng. J. 421 (2021) 129689.
[106] M. Tang, S. Zhang, S. Chen, Chem. Soc. Rev. 51 (2022) 1529–1546.
[107] E. Ogungbemi, T. Wilberforce, O. Ijaodola, J. Thompson, A.G. Olabi, J. Hydrogen Energy 46 (2021) 30625–30640.
[108] L. Xing, W. Xiang, R. Zhu, Z. Tu, Int. J. Hydrogen Energy 47 (2022) 1888–1900.
[109] J. Zhang, B. Hu, X. Deng, C. Li, Y. Wu, C. Zhou, D. Zhang, L. Ge, W. Zhou, Z. Shao, ACS Appl. Mater. Interfaces 14 (2022) 30872–30880.
[110] H. Cheng, R. Gui, H. Yu, C. Wang, S. Liu, H. Liu, T. Zhou, N. Zhang, X. Zheng, W. Chu, Y. Lin, H. Wu, C. Wu, Y. Xie, Pest. Artic. News Summ. 118 (2021) e2104026118.
[111] K. Dong, Y. Lei, H. Zhao, J. Liang, P. Ding, Q. Liu, Z. Xu, S. Lu, Q. Li, X. Sun, J. Mater. Chem. A 8 (2020) 23123–23141.
[112] R.K. Nekouei, S.S. Mofarah, S. Maroufi, C. Cazorla, A.P. O'Mullane, Y. Yao, S. Lim, A. Tricoli, V. Sahajwalla, J. Mater. Chem. A 9 (2021) 26727–26740.
[113] X. Hu, Z. Sun, G. Mei, X. Zhao, B.Y. Xia, B. You, Adv. Energy Mater. 12 (2022) 2201466.
[114] M. Qin, S. Fan, L. Wang, G. Gan, X. Wang, J. Cheng, Z. Hao, X. Li, J. Colloid Interface Sci. 562 (2020) 540–549.
[115] P. Cao, X. Quan, K. Zhao, X. Zhao, S. Chen, H. Yu, ACS Catal. 11 (2021) 13797–13808.
[116] Y. Wang, R. Shi, L. Shang, L. Peng, D. Chu, Z. Han, G.I.N. Waterhouse, R. Zhang, T. Zhang, Nano Energy 96 (2022) 107046.
[117] X. Zhang, X. Zhao, P. Zhu, Z. Adler, Z. Wu, Y. Liu, H. Wang, Nat. Commun. 13 (2022) 2880.
[118] C. Xiao, L. Cheng, Y. Zhu, G. Wang, L. Chen, Y. Wang, R. Chen, Y. Li, C. Li, Angew. Chem. Int. Ed. 61 (2022) e202206544.
[119] Z. Wang, C. Wang, Y. Hu, S. Yang, J. Yang, W. Chen, H. Zhou, F. Zhou, L. Wang, J. Du, Y. Li, Y. Wu, Nano Res. 14 (2021) 2790–2796.
[120] X. Tan, C. Yu, Y. Ren, S. Cui, W. Li, J. Qiu, Energy Environ. Sci. 14 (2021) 765–780.
[121] Y. Li, N.M. Adli, W. Shan, M. Wang, M.J. Zachman, S. Hwang, H. Tabassum, S. Karakalos, Z. Feng, G. Wang, Y. Li, G. Wu, Energy Environ. Sci. 15 (2022) 2108–2119.
[122] W. Ren, X. Tan, C. Jia, A. Krammer, Q. Sun, J. Qu, S.C. Smith, A. Schueler, X. Hu, C. Zhao, Angew. Chem. Int. Ed. 61 (2022) e202203335.
[123] J. Yi, X. Gao, H. Zhou, W. Chen, Y. Wu, Angew. Chem. Int. Ed. 61 (2022) e202212329.
[124] W. Ma, S. Xie, T. Liu, Q. Fan, J. Ye, F. Sun, Z. Jiang, Q. Zhang, J. Cheng, Y. Wang, Nat. Catal. 3 (2020) 478–487.
[125] M. Zheng, P. Wang, X. Zhi, K. Yang, Y. Jiao, J. Duan, Y. Zheng, S. Qiao, J. Am. Chem. Soc. 144 (2022) 14936–14944.
[126] Y. Zhao, X. Zu, R. Chen, X. Li, Y. Jiang, Z. Wang, S. Wang, Y. Wu, Y. Sun, Y. Xie, J. Am. Chem. Soc. 144 (2022) 10446–10454.
[127] J.Y.T. Kim, P. Zhu, F. Chen, Z. Wu, D.A. Cullen, H. Wang, Nat. Catal. 5 (2022) 288–299.
[128] N. Muradov, Int. J. Hydrogen Energy 42 (2017) 14058–14088.
[129] S. Wu, N. Salmon, M.M.J. Li, R. Bañares-Alcántara, S.C.E. Tsang, ACS Energy Lett. 7 (2022) 1021–1033.
[130] G. Soloveichik, Nat. Catal. 2 (2019) 377–380.
[131] Small-scale green ammonia plants open up new storage possibilities for wind and solar power. https://insights.thyssenkrupp-industrial-solutions.com/story/small-scale-green-ammonia-plants-open-up-new-storage-possibilities-for-wind-and-solar-power/.
[132] Siemens develops world's first energy storage demonstrator to deliver carbon free power of the future. https://news.siemens.co.uk/news/siemens-develops-world-s-first-energy-storage-demonstrator-to-deliver-carbon-free-power-of-the-future.
[133] F. Chang, W. Gao, J. Guo, P. Chen, Adv. Mater. 33 (2021) 2005721.
[134] G. Jeerh, M. Zhang, S. Tao, J. Mater. Chem. A 9 (2021) 727–752.
[135] D.R. Macfarlane, P.V. Cherepanov, J. Choi, B.H.R. Suryanto, R.Y. Hodgetts, J.M. Bakker, F.M.F. Vallana, A.N. Simonov, Joule 4 (2020) 1186–1205.
[136] L. Zhai, C.S. Wong, H. Zhang, P. Xiong, X. Xue, Y.L. Ho, C. Xu, Y.C. Fong, J. Mei, W.W. Chan, S.C. Ip, S. Niu, S.P. Lau, K.W.E. Cheng, M.M.J. Li, Chem. Eng. J. 452 (2023) 139390.
[137] Y. Yuan, L. Zhou, H. Robatjazi, J.L. Bao, J. Zhou, A. Bayles, L. Yuan, M. Lou, M. Lou, S. Khatiwada, E.A. Carter, P. Nordlander, N.J. Halas, Science 378 (2022) 889–893.